



OPEN ACCESS

EDITED BY

Anna Schneider,
Brandenburg University of Technology
Cottbus-Senftenberg, Germany

REVIEWED BY

Hema Achyuthan,
Anna University, India
Daisy Valera-Fernández,
National Autonomous University of
Mexico, Mexico

*CORRESPONDENCE

Alireza Karimi,
✉ karimi-a@um.ac.ir

RECEIVED 30 January 2023

ACCEPTED 16 May 2023

PUBLISHED 25 May 2023

CITATION

Bayat O, Karimi A, May J-H, Fattahi M,
Wiesenberg GLB and Egli M (2023), High-
resolution record of stable isotopes in soil
carbonates reveals environmental
dynamics in an arid region (central Iran)
during the last 32 ka.

Front. Earth Sci. 11:1154544.

doi: 10.3389/feart.2023.1154544

COPYRIGHT

© 2023 Bayat, Karimi, May, Fattahi,
Wiesenberg and Egli. This is an open-
access article distributed under the terms
of the [Creative Commons Attribution
License \(CC BY\)](https://creativecommons.org/licenses/by/4.0/). The use, distribution or
reproduction in other forums is
permitted, provided the original author(s)
and the copyright owner(s) are credited
and that the original publication in this
journal is cited, in accordance with
accepted academic practice. No use,
distribution or reproduction is permitted
which does not comply with these terms.

High-resolution record of stable isotopes in soil carbonates reveals environmental dynamics in an arid region (central Iran) during the last 32 ka

Omid Bayat^{1,2}, Alireza Karimi^{1*}, Jan-Hendrik May³,
Morteza Fattahi⁴, Guido L. B. Wiesenberg² and Markus Egli²

¹Department of Soil Science, Faculty of Agriculture, Ferdowsi University of Mashhad, Mashhad, Iran,

²Department of Geography, University of Zurich, Zurich, Switzerland, ³School of Geography, University of Melbourne, Melbourne, VIC, Australia, ⁴Institute of Geophysics, University of Tehran, Tehran, Iran

Although central Iran is pivotal for palaeoclimatic correlations, palaeoenvironmental data for this region is very sparse and a reliable chronology for pedogenic features is lacking. We therefore tried to answer the question how the environmental conditions and, in particular, the climate developed over time by using the isotopic signatures of pedogenic carbonates. We present a chronology of pedogenic carbonates in association with stable carbon and oxygen isotopes in both the matrix and coating carbonates of a relict palaeosol (Baharan palaeosol) in central Iran to understand the dynamics of environmental changes in this region during the late Quaternary. The palaeosol experienced several episodes of leaching during pedogenesis as reflected in its morphology (carbonate coatings under the rock fractions) and geochemical characteristics (Ba/Sr ratios). The $\delta^{18}\text{O}$ values of both the matrix and coating carbonates in the upper 60 cm (especially in the upper 20 cm) of the pedon are enriched ($\sim 4\text{‰}$) compared to the subsoil and are mainly related to the impact of evaporation. Moreover, the $\delta^{13}\text{C}$ values of the carbonates are in isotopic disequilibrium with the modern vegetation cover (desert shrubs) of the study area and are enriched in different degrees. The carbonates in the top 60 cm are formed by the input of atmospheric CO_2 and calcareous dust while deeper carbonates formed in an environment exhibiting a higher contribution of C_4 plants. Based on the radiocarbon chronology of carbonate coatings, it seems that three main stages of palaeoenvironmental changes occurred in the region during the last 32 ka. The first stage lasted ca. 5,000 years (between 31.6 and 26.0 ka) and was accompanied by deep leaching under sub-humid climatic conditions and the expansion of C_4 plants. Under the dominance of semi-arid conditions during the second stage until the late Holocene, a gradual increase in the $\delta^{18}\text{O}$ values and aridity occurred in the region. The last phase in the late Holocene was characterised by the establishment of an arid and evaporative environment with a sparse vegetation cover. A climatic correlation using the oxygen isotopic composition of secondary carbonates from the Baharan palaeosol, Soreq Cave (the Levant) and Hoti Cave (Oman; both having speleothems records) suggested a climatic connection between central Iran and the eastern Mediterranean during the late Pleistocene and between central Iran and northern Oman during the late Holocene.

KEYWORDS

relict palaeosols, pedogenic carbonates, carbonate coatings, carbon and oxygen isotopes, radiocarbon chronology, late quaternary, paleoclimate, western Asia

1 Introduction

Soil carbonates are an important component of terrestrial ecosystems because they are a sink of carbon over geological times (Monger, 2014; Shariffar et al., 2023), preserve records of palaeoenvironmental changes (Monger et al., 1998; Pustovoytov, 1998; Pustovoytov, 2003; Retallack, 2005; Achyuthan et al., 2007; Shankar and Achyuthan, 2007; Ebeling et al., 2016; Oerter et al., 2016; Bayat et al., 2018; Bayat et al., 2021; Zhou et al., 2021; Fernández et al., 2022) and provide a geochronological tool for both relative (Machette, 1985; Bayat et al., 2018) and absolute dating (Amundson et al., 1994; Pendall et al., 1994; Pustovoytov, 1998; Pustovoytov, 2003; Dal Sasso et al., 2018) of landforms and archaeological sites (Pustovoytov, 2003; Dal Sasso et al., 2018). Climate is the most important factor for the formation of pedogenic carbonates (Machette, 1985; Zamanian et al., 2016) and controls their accumulation rates (Amundson et al., 1989; Pustovoytov, 2003) and their geochemistry (Cerling, 1984; Cerling and Quade, 1993; Bayat et al., 2018). Pedogenic carbonate forms in the soil environment usually through the translocation of bicarbonate ions and deposition of calcite mineral (calcification process) over geologic times (Machette, 1985; Birkeland, 1999; Monger, 2014). Generally, net water deficit and incomplete leaching of soils in arid and semi-arid regions are the main causes of carbonate deposition in the pedon (Cerling and Quade, 1993; Amundson, 2005; Dal Sasso et al., 2018). In addition, rapid evaporation, degassing and soil freezing can accelerate the formation of secondary carbonates (Cerling, 1984; Sheldon and Tabor, 2009; Gocke et al., 2011; Zamanian et al., 2016).

The application of stable isotopic geochemistry of pedogenic carbonates over the last 4 decades has proven its reliability as an environmental tracer for studies of earth surface processes and also as an indicator of shifts in palaeoenvironmental conditions (e.g., Cerling, 1984; Amundson et al., 1989; Andrews et al., 1998; Ebeling et al., 2016; Bayat et al., 2018; Bayat et al., 2021; Fernández et al., 2022). The oxygen isotope composition of pedogenic carbonate is related to climatic parameters (local meteoric water, crystallization temperatures and evaporative rates) while stable carbon isotope values of pedogenic carbonates are linked to the carbon cycle and controlled by the isotopic composition of soil CO₂ that is determined itself by the composition of the local ecosystems and metabolic pathway of plants (C₃, C₄, Crassulacean acid metabolism (CAM) plants), soil respiration rates and the influx of atmospheric CO₂ near the soil surface (Cerling, 1984; Amundson et al., 1989; Cerling and Quade, 1993; Quade, 2014). Where pollen assemblages are absent, soil carbonates and their δ¹³C values provided hints to the development of palaeo-vegetation and photosynthetic pathways in arid/hyper-arid deserts of the Thar (Andrews et al., 1998; Achyuthan et al., 2007), Atacama (Ebeling et al., 2016), Negev desert (Amit et al., 2017) and central Iran (Bayat et al., 2018). However, caution must be exercised when interpreting palaeoenvironmentals from

the isotopic composition of soil carbonates because of a potential contamination with detrital carbonates (especially in soils with calcareous parent materials) (Amundson et al., 1989) or recrystallisation processes (Pendall et al., 1994; Budd et al., 2002) which can easily destroy the palaeoclimatic evidence of soil carbonates. The input of calcareous dust can result in a change of the isotopic composition of pedogenic carbonates indicating an increase in environmental aridity and wind erosion. Furthermore, soil carbonates formed around deep-rooting plants can alter the chronology of syngenetic carbonate of palaeosols (Gocke et al., 2014). Moreover, recent studies have emphasised a seasonal bias in the formation of soil carbonates (Breecker et al., 2009; Kelson et al., 2020; Railsback, 2021; Sarangi et al., 2021; Domínguez-Villar et al., 2022). Therefore, palaeoclimatic signatures of soil carbonates may rather indicate the conditions of a particular part of the year than average annual parameters.

The arid bioclimatic zone is the most extensive region in western Asia and Iran (Goudie, 2013). It is generally believed that arid ecosystems are very sensitive to climatic variations, human activities and desertification processes (Goudie, 2013; Yanes et al., 2019; Khosravichenar et al., 2020). Thus, the identification of past climatic changes can highlight the natural ranges, rates and dynamics of climatic variability in arid regions (Goudie, 2013; Yanes et al., 2019; Tierney et al., 2020).

Although the Middle East is one of the global hot-spots of climate change (Giorgi, 2006) and water scarcity menaces the socioeconomic development of the region (Jones et al., 2019; Shoaee et al., 2023), palaeoclimatic records required for a better understanding of natural climatic variability are very limited (Flohr et al., 2017; Jones et al., 2019). Arid regions of central Iran are also important as a key region for palaeoclimatic correlations between Europe and central Asia, the identification of atmospheric shifts over western Asia during the late Quaternary (Thomas et al., 1997; Rashidi et al., 2022) and the determination of hominin pathways from southwestern Asia to central Asia (Shoaee et al., 2023). Owing to the abundant historical and pre-historical settlements in the central plateau of Iran, this region is a suitable place to examine the role of climatic changes (especially during the Holocene) on the development and collapse of ancient civilizations of the Middle East (Schmidt et al., 2011; Petrie and Weeks, 2019). Although long-term climatic data are a prerequisite to assess the role of natural climatic variability on dryland-landscape dynamics (Bradley, 2015; Yanes et al., 2019), only very sparse data exist on the palaeoenvironment of central Iran. The pedogenic development of soils in arid regions of central Iran has been subject of several studies, but these investigations mostly lack a reliable chronology (e.g., Khademi and Mermut, 1999) or only present relative ages of landforms (e.g., Bayat et al., 2018) or numerical dating of the parent material of the soils (e.g., Rashidi et al., 2022).

Here, we present new chronological data from pedogenic carbonates in an arid region in eastern Isfahan, central Iran, in



FIGURE 1

Investigation area with the Baharan palaeosol profile and the Zayandehroud river (source: Google Earth).

association with detailed values of oxygen and carbon isotopes (for both matrix and coating carbonates) to understand the dynamics of environmental changes in the region during the late Quaternary. Our main research question was: How and when did the environmental conditions and in particular the temperature-precipitation regime change since the Late Pleistocene based on isotopic signatures ($\delta^{13}\text{C}$, $\delta^{18}\text{O}$) in pedogenic carbonates?

2 Environmental settings

2.1 Geology and geomorphology

The study area is located in central Iran, western Asia ($32^{\circ}26'\text{N}$, $52^{\circ}06'\text{E}$, Figure 1). It comprises eastern Isfahan and the western part of the Gavkhoni Playa. The playa is the terminal point of the Zayandehrud River which starts from the Zagros Mountains. The interactions of tectonic movements and climatic changes during the late Tertiary and Quaternary shaped the structure of the Zayandehrud Valley. The variation of environmental factors led to changes in fluvial processes of the Zayandehrud River and its tributaries, lake levels of the Gavkhoni Playa and changes in aeolian processes giving rise to a complex landscape comprising diverse landforms and soils in eastern Isfahan (Shlemon, 1978; Bayat, 2007; Ghaiumi Mohammadi, 2011). Geologically, most of eastern Isfahan is covered by Quaternary alluvium while Cretaceous limestone and Jurassic shale are the dominant bed rocks in the mountains of the region (Zahedi, 1976).

2.2 Bioclimatic conditions

According to 23 years of meteorological observations (1992–2015) at the Kaboutarabad station, the nearest

meteorological station to the study area, the climate is arid to hyper-arid and the area receives rainfall over a period of 6 months beginning in November. The mean annual temperature is roughly 17.8°C , average annual rainfall is around 107 mm with a high potential evaporation (2052 mm yr^{-1}) indicating a severe water deficit in the region. The depth of soil leaching in the eastern Isfahan region is negligible (Bayat et al., 2018) and reaches a maximum of about 5 cm (Shlemon, 1978).

The $\delta^{18}\text{O}$ values of meteoric water (influenced by the isotopic values of water vapour in clouds and the impact of condensation processes (Hoefs, 2021)) in the study area vary seasonally and have an annual average of about -7‰ according to Standard Mean Ocean Water (SMOW) (Bowen, 2017). In general, western Asia has among the highest values in Asia (Supplementary Figure S1) and the world (Gat, 1996; Bowen, 2017). There is a very strong and positive correlation ($r = +0.983$, Supplementary Figure S2) between modern monthly air temperature and the $\delta^{18}\text{O}$ values of meteoric water (temperature effect) in the study area demonstrating the dominant role of westerlies and cool-season rainfalls (Kutzbach et al., 2014).

The soil temperature regime of the area is thermic with a mean annual temperature of 17.9°C at a depth of 50 cm (Bagheri, 2005). The distribution of soil temperature at different depths of the Kaboutarabad station is given in Supplementary Figure S3. The soils of the study area are classified as Aridisols. Previous studies showed that regional soils are mainly characterised by cambic, gypsic, calcic and argillic horizons (Khademi and Mermut, 1999; Bayat, 2007; Ghaiumi Mohammadi, 2011; Bayat et al., 2017; Bayat et al., 2018).

The current flora of the study areas is a mixture of C_3 shrubs and C_4 grasses, with a dominance of C_3 plant desert shrubs. The $\delta^{13}\text{C}$ value of organic materials in the soils of the region is -22.5‰ relative to the Pee Dee Belemnite (PDB) standard (Khademi and Mermut, 1999; Bayat, 2007). The most important native plants are *Artemisia Sieberia* L., *Scariolaorientalis* Boiss., *Launea spinosa* Forsk., *Euphorbia gedrosiaca*, *Anabasis aphylla* L., *Noeamucronata* and *Salsola nitraria* (Khademi and Mermut, 1999).

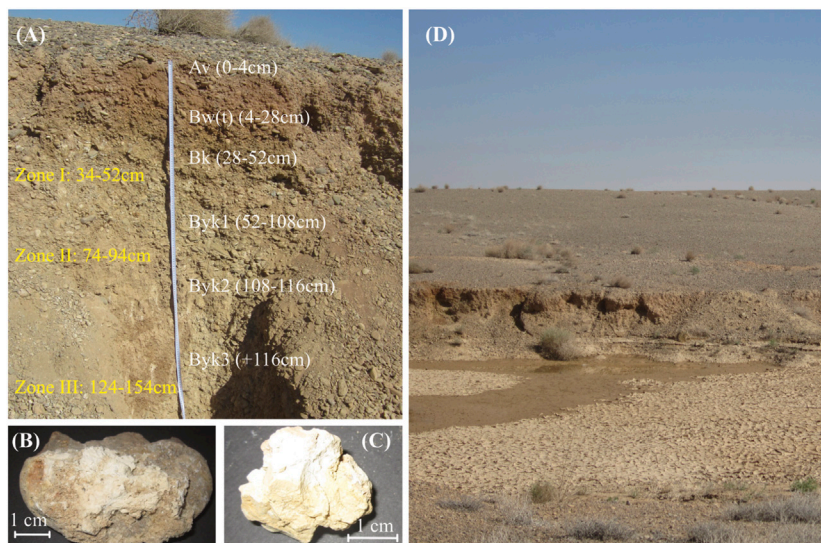


FIGURE 2

(A) Profile characteristics of the Baharan palaeosol (B) carbonate coatings underside of a clast (C) an interpebble nodule in the profile and (D) image of the landscape at Baharan.

2.3 The Baharan palaeosol

Palaeoenvironmental changes during the late Tertiary and early-mid Quaternary in the Zayandehrud River valley shaped the landscape of the region (Shlemon, 1978; Saadatmand, 1999; Bayat, 2007; Ghaiumi Mohammadi, 2011). The upper terraces are relicts of an old landscape and are widely distributed in the eastern Isfahan region (Figure 1). These landforms are characterised by uplifted and dissected features, flat surfaces (slope $\sim 0.4\%$) and a gravelly structure near the surface (Shlemon, 1978; Bayat, 2007). The Baharan area is situated between the Gharneh alluvial fan and the Zayandehrud River (Figure 1). Previous stratigraphic studies in eastern Isfahan have shown that the late Quaternary alluvium of these landforms covers thick silty-marly sediments of the Plio-Pleistocene (Shlemon, 1978; Bayat, 2007). Secondary processes altered the top gravel-layer through accumulation of dust (vesicular horizons) as well as pedogenic processes such as calcification and gypsification (Saadatmand, 1999; Bayat, 2007).

The Baharan palaeosol is located at an elevation of 1,540 m. a.s.l. The profile can be divided into two separate parts, a non-gravelly vesicular horizon and a relict and gravelly palaeosol (Figure 2). A thin (~ 4 cm) vesicular horizon is overlying the gravelly skeleton indicating the accumulation of recent dust material at the surface of the palaeosol (Amit et al., 2017).

The surface of the terrace is flat and, thus, the section and its palaeosol remained safe from erosional processes.

The relatively flat and stable topography and the hydrological isolation from groundwater and/or adjacent landforms provide suitable conditions for the reconstruction of climate and its effects on the environment (Birkeland, 1999; Amit et al., 2017). In combination with the good permeability of the alluvial sediment that build up the terrace, the Baharan palaeosol therefore provides an excellent opportunity to decipher palaeoclimatic conditions in this area.

3 Methods and materials

3.1 Fieldwork and sampling

The description of the morphology of the palaeosol was done according to Schoeneberger et al. (2012) and the stages of the morphological development of pedogenic carbonates were assessed using the morphological models of Netterberg (1971); Netterberg (1978) and Machette (1985). A high-resolution strategy was used for sampling and around 2 kg of soil material were taken from each 10 cm interval depth. Furthermore, samples were taken from vesicular materials at the surface of the palaeosol and also from coating-bearing pebbles. The outer part of soil carbonate nodules or coatings can be subjected to recrystallisation and/or gypsum solution and re-precipitation. This may influence the stable isotope ratios. Therefore, we used the inner part of carbonates for the isotope analyses.

3.2 Laboratory analyses

The bulk samples were sieved to obtain the gravel (>2 mm) and fine earth (<2 mm) fraction, and the weight contents were registered. The gravel was free of gypsum coatings.

Chemical properties of the soil samples (including pH, electrical conductivity (EC), organic carbon, calcium carbonate equivalent gypsum content) were determined for the fine earth fraction using standard methods (Soil Survey Staff, 2014). The total elemental contents were measured by using an energy dispersive XRF spectrometer (XRF; SPECTRO X-LAB 2000; SPECTRO Analytical Instruments, Germany). About 5–6 g of milled fine earth was analysed as loose powder. A soil standard (NCS DC 73326) was used for quality control. For strontium, barium and rare earth elements contents, inductively coupled plasma mass spectrometry (ICP-MS) was used.

The $\delta^{13}\text{C}$ and $\delta^{18}\text{O}$ ratio of the soil material and carbonates were determined using elemental analysis isotope ratio mass spectrometry (EA-IRMS; Thermo Fisher Scientific Flash HT Plus elemental analyser equipped with a thermal conductivity detector and coupled to a ConFloV to Delta V Plus isotope ratio mass spectrometer). The isotopic values were calculated using in-house standards (Caffeine (Sigma), Chernozem (Black Carbon Reference Materials)) that were calibrated with international reference materials (Caffeine (IAEA 600), Benzoic acid (IAEA 601), Cellulose (IAEA CH3), ammonium sulphate (IAEA N1) and Urea (IVA)). The carbonate content was determined according to Breitenbach and Bernasconi (2011, slightly modified method) using a CTA PAL autosampler and GasBench-IRMS (Thermo Fisher Scientific GasBench II coupled to Delta V Plus IRMS). Aliquots of samples and standards (20–100 μg carbonate C) were weighed into vials, closed and automatically flushed with He for 10 min 25–50 μL phosphoric acid was added and the samples were measured at least 60 min after acid addition (Breitenbach and Bernasconi, 2011). The carbonate C content and $\delta^{13}\text{C}$ and $\delta^{18}\text{O}$ values were calibrated against a secondary standard (Merck CaCO_3) and international reference material (IAEA NBS18 Calcite).

Isotope data presented here are the average of triple measurements for each sample and are reported in delta (δ) notation relative to the standards for C and O (Coplen, 1988; Coplen et al., 2006; Hoefs, 2021):

$$\delta(\text{‰}) = \left(\frac{R_{\text{Sample}}}{R_{\text{Standard}}} - 1 \right) \times 1000 \quad (1)$$

Where R is the ratio of heavy isotopes to light ones ($^{13}\text{C}/^{12}\text{C}$ or $^{18}\text{O}/^{16}\text{O}$) in samples and standard.

A reconstruction of palaeovegetation was tentatively done by using the stable carbon isotopic values and the following equations (Cerling and Quade, 1993; Sarangi et al., 2021):

$$C_4(\%) = \left(\frac{11.9 + \delta^{13}\text{C}_{\text{sample}}}{14} \right) \times 100 \quad (2)$$

The percentage of the contribution of atmospheric CO_2 to the $\delta^{13}\text{C}$ of the soil carbonates was calculated using a linear mass balance model:

$$\text{CO}_2(\%) = \left(\frac{\delta^{13}\text{C}_{\text{sample}} - \delta^{13}\text{C}_{\text{bio}}}{\delta^{13}\text{C}_{\text{CO}_2} - \delta^{13}\text{C}_{\text{bio}}} \right) \times 100 \quad (3)$$

Where $\delta^{13}\text{C}_{\text{sample}}$ is the carbon isotopic value of the pedogenic carbonate after enrichment corrections (Cerling, 1984), $\delta^{13}\text{C}_{\text{bio}}$ is the carbon isotopic value of biologically-produced CO_2 in the soils of the study area (-22.5‰ , PDB (mean of $\delta^{13}\text{C}$ of native plants in the region)) and $\delta^{13}\text{C}_{\text{CO}_2}$ is the $\delta^{13}\text{C}$ value of atmospheric CO_2 acquired from ice cores for the period of carbonate genesis.

For radiocarbon dating, the carbonate of 8 samples was dissolved by applying 10% HCl and the CO_2 trapped. The samples were heated under vacuum in quartz tubes with CuO (oxygen source) to remove any absorbed CO_2 in the CuO. The tubes were then evacuated again, sealed and heated in the oven at 900°C to obtain CO_2 . The CO_2 of the combusted sample was mixed with H_2 (1:2.5) and catalytically reduced over iron powder at 535°C to elemental carbon (graphite). After reduction, the mixture was pressed into a target and carbon ratios measured by Accelerator

Mass Spectrometry (AMS) using 0.2 MV radiocarbon dating facility (MICADAS) of the Ion Beam Physics at the Swiss Federal Institute of Technology Zurich (ETHZ). The calendar ages were obtained using the OxCal 4.4 calibration program (Bronk Ramsey, 2001; Bronk Ramsey, 2009; Reimer, 2020) by applying the IntCal 20 calibration curve and for modern samples the Bomb 21NH3 curve (Hua et al., 2013; Reimer et al., 2013) is used. Calibrated ages are given in the 1σ and 2σ range (minimum and maximum value for each).

3.3 Palaeoprecipitation estimation using a Bk-Depth climofunction

To evaluate palaeoprecipitation, the equation derived by a global climofunction and described by Retallack (2005) was used:

$$MAP = 137.24 + 6.45D - 0.013D^2 \quad (4)$$

Where MAP is the mean annual precipitation (mm) and D is the depth to the upper boundary of a Bk horizon (cm). This equation is valid for MAP values up to about 1000 mm (Beverly et al., 2018). The thickness of a thin layer (~ 4 cm) of dust-derived sediment is not considered in the calculations.

4 Results

4.1 Morphology and physicochemical properties

The pedogenetic properties of the Baharan profile are presented in Figure 2A and exhibit two distinct parts along the profile. In the upper part, a thin layer of vesicular material (Av) has accumulated. Below this material, a red/argillic horizon and a calcic horizon are present. The lower part of the pedon is a succession of gypsic-calcic (Byk) horizons. The palaeosol is characterised by a sandy loam texture along the pedon. The exception is the vesicular horizon at the surface that has a loamy texture.

The profile is characterised by a high content of rock fragments (Figure 3A). In general, a surface layer having a low gravel content can be observed followed by highly to very highly gravelly layers (Figure 3B). The soil material has a homogenous geochemical composition rich in silica, alumina and iron (Figure 3C).

The Baharan palaeosol is a non-saline palaeosol in which the EC values vary between 0.15 dS m^{-1} in the upper part to 2.37 dS m^{-1} in the lower part (Table 1). The non-saline nature of this soil in an arid and evaporative environment is owing to the lack of a saline-shallow groundwater, saline dust input and the free drainage of the soil. The palaeosol had near-neutral pH values (7.41–7.92), mainly controlled by the abundance of carbonates (Birkeland, 1999). As expected for a soil in an arid region, the organic carbon content is very low and varies between 0.01%–0.11%. It is even lower than in other palaeosols of an adjacent alluvial fan (Gharneh alluvial fan, Figure 1) described by Bayat et al. (2018).

In the Baharan soil profile, the carbonate coatings accumulated at depths of 34–52 (zone 1), 74–94 (zone 2) and 124–154 cm (zone 3) (Figure 2A). In zone 1, carbonates accumulated at the bottom of the clasts while in zone 2 and 3 carbonate coatings were on the top

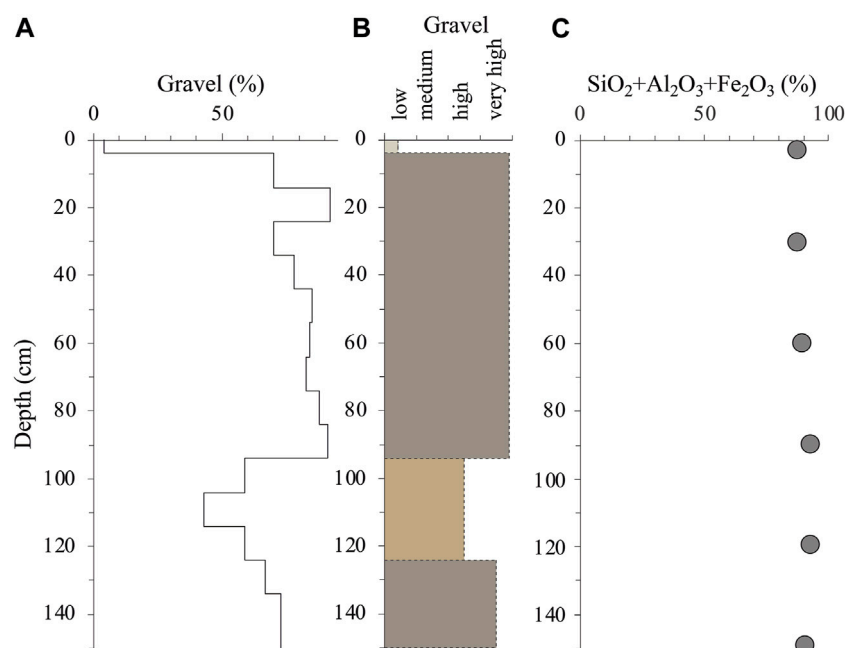


FIGURE 3

(A) Gravel content (B) sediment log of the Baharan palaeosol profile (the distinction of the layers is based on the gravel content) and (C) main elements concentration (as oxides) of the clast fraction in the soil profile.

and underside of the clasts (Figure 2B). These conditions indicate the movement of water in gravelly soils. The deposition of calcite occurred on the warmer sides of clasts and pebbles (Amundson et al., 1997). Inter-pebble hard nodules also accompany carbonate coatings especially in zones 2 and 3. These nodules are creamy white with an irregular shape and diameter of about 3 cm (Figure 2C). The morphology and developmental stages of pedogenic carbonates provides valuable information about the formation processes and relative ages of soils and associated landforms Netterberg (1971) and Netterberg (1978); Machette (1985)). Netterberg's approach is based on landforms of the southern African region using a 6-class model for the morphology of secondary carbonates in weathered rocks, shattered clay, mixed texture materials and sand/gravels. Machette (1985) suggested also a 6-class model for secondary carbonates in gravelly and non-gravelly materials by studying landforms of southwestern United States. The morphology of the carbonates in the Baharan palaeosol (coalesced coatings and inter-pebble nodules) indicates that they are in an incipient stage of development (stage 1 according to Netterberg (1971); Netterberg (1978) and stage II-III of Machette's (1985) morphological model). Regarding the morphology of carbonates and the lithology of host clasts (non-calcareous clasts), these carbonates are undoubtedly of pedogenic origin (Machette, 1985; Amundson et al., 1997; Pustovoytov, 2003).

The palaeosol also have gypsiferous characteristics: Three major zones of gypsum accumulation were identified, i.e., at the depths of ~50–75 cm, ~90–115 cm and ~130–155 cm. The gypsum content varied between 0.69% and 6.03% (Table 1) and gypsum occurred as coatings (rinds, pendants) on the underside of gravels and also on the surface of carbonate coatings.

Since the rock fragment characteristics and amount significantly influenced the development traits and geochemistry of pedogenic carbonates (Machette, 1985; Pustovoytov, 1998; Pustovoytov, 2003), the properties of the clast fractions of the palaeosol were examined. The profile is very gravelly and contains between 43 and 92 weight-% rock fragments (Table 1). Geochemically, SiO_2 , Al_2O_3 and Fe_2O_3 are the major components of the clast fraction and exhibit a relatively uniform distribution along the pedon (Figure 3C). Therefore, the clast fraction of the pedon is non-calcareous.

4.2 Geochemical indices of leaching, calcification and soil carbonates

Leaching (Ba:Sr ratio) and calcification ($(\text{CaO} + \text{MgO})/\text{Al}_2\text{O}_3$ ratio) indices are plotted in Figures 4A, B. Sr and Ba have similar atomic properties; while Sr has a higher solubility than Ba. Therefore, the Ba/Sr ratio is an index of the leaching behaviour during pedogenesis (Sheldon, 2006; Sheldon and Tabor, 2009; Zhou et al., 2021). The leaching index of the Baharan soil profile represents three major zones of leaching at depths ~30 cm, ~80 cm and ~130 cm (Figure 4A) with a maximum value near the surface (Ba/Sr = ~0.5) that corresponds to the Bt horizon of the pedon (Figure 4A). Several leaching periods in the palaeosol can thus be interpreted. Since previous studies demonstrated that the amount of rainfall is a critical factor in controlling the depth of soil leaching (Egli and Fitze, 2001), these leaching events are related to an increase in regional precipitation in the past.

The calcification index exhibits four major zones of carbonation at depths of around 40 cm, between 70 and 90, 120 and ~150 cm

TABLE 1 Selected chemical and geochemical properties of the Baharan palaeosol.

Sample code	Depth (cm)	Horizon	Dry Munsell colour	pH (H ₂ O)	pH (CaCl ₂)	EC ^a (dS m ⁻¹)	Gravel	Gypsum	OC ^b	CCE ^c	Secondary carbonates ^d	CaO		MgO		Ba		Sr	
												%				g kg ⁻¹		mg kg ⁻¹	
S1	0–4	Av	10YR 6/4	7.82	7.63	1.13	5.4	0.77	0.08	39.8	-	156.5	50.4	270	430				
S2	4–14	Bw(t)	7.YR 5/4	7.87	7.62	0.45	70	1.68	0.10	34.0	-	183.0	38.6	215	397				
S3	14–24		7.5YR 5/4	7.75	7.39	0.73	92	0.99	0.08	35.0	-	161.4	42.4	195	371				
S4	24–34	Bk	7.5YR 5/6	7.83	7.66	0.15	70	0.75	0.11	37.0	-	169.6	33.5	308	393				
S5	34–44		10YR 5/6	7.86	7.64	0.68	78	1.08	0.09	40.9	83.2	176.6	31.4	193	605				
S6	44–54		10YR 5/6	7.92	7.74	0.56	85	0.73	0.08	31.1	75.4	187.9	26.9	189	1,042				
S7	54–64	Bky1	10YR 6/4	7.60	7.43	2.21	84	6.04	0.08	21.0	-	164.0	24.7	184	3,617				
S8	64–74		10YR 6/4	7.49	7.58	2.32	83	5.73	0.08	27.9	-	203.6	21.7	181	2,855				
S9	74–84		10YR 6/4	7.26	7.45	2.22	88	1.58	0.05	22.6	79.7	179.9	22.2	175	1,318				
S10	84–94		10YR 6/4	7.62	7.41	2.15	91	1.75	0.07	26.5	49.5	172.0	22.3	166	1,285				
S11	94–104		10YR 6/4	7.52	7.67	2.37	59	3.14	0.07	24.8	-	187.1	22.1	141	1,242				
S12	104–114	Bky2	10YR 7/4	7.49	7.70	2.29	43	2.01	0.04	27.3	-	204.0	24.5	128	1,174				
S13	114–124		10YR 7/4	7.62	7.39	2.18	59	0.70	0.08	29.0	-	233.2	24.0	119	915				
S14	124–134	Bky3	10YR 7/4	7.62	7.60	2.23	67	0.81	0.01	32.3	59.5	221.2	22.1	135	584				
S15	134–144		10YR 7/4	7.53	7.54	2.19	73	2.93	0.04	35.5	33.7	208.4	22.7	147	1715				
S16	144–154		10YR 7/4	7.51	7.48	2.22	77	2.00	0.08	33.8	33.6	215.9	23.2	135	1,281				

^aEC: Electrical conductivity.^bOC: Organic carbon.^cCCE: Calcium carbonate equivalent.^dSecondary carbonates: carbonates on clasts, nodules.

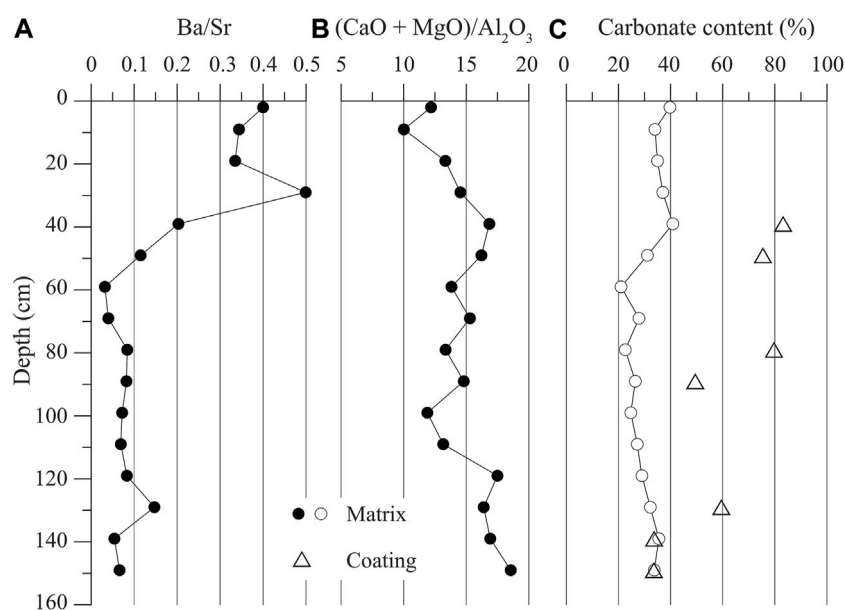


FIGURE 4 (A) Geochemical leaching index (Ba/Sr) (B) calcification index (CaO+MgO)/Al₂O₃ and (C) carbonate content of the matrix (circles) and coatings (triangles) of the Baharan palaeosol.

TABLE 2 Radiocarbon ages of carbonate coatings.

Sample ID	UZ No.	Depth (cm)	¹⁴ C age	±1σ	F14C	±1σ	δ ¹³ C (‰)	±1σ	Calibrated ages (cal BP)	
			(a BP)					1σ-range	2σ-range	
PC 1	6,864	39	16432	70	0.129	0.0011	-0.9	1	19921–19624	20045–19582
PC 2	6,865	49	8,115	33	0.364	0.0015	0.7	1	9,089–9,000	9,133–8,990
PC 3	6,866	79	24769	181	0.046	0.0010	-2.7	1	29156–28832	29447–28614
PC 4	6,867	89	22234	135	0.063	0.0011	-5.8	1	26891–26331	26964–26065
PC 5	6,868	129	25354	193	0.043	0.0010	-1.5	1	29891–29323	30001–29210
PC 6	6,869	139	25727	201	0.041	0.0010	0.0	1	30231–29862	30383–29317
PC 7	6,870	149	26981	236	0.035	0.0010	-3.5	1	31255–30960	31604–30790

(Figure 4B) which is in agreement with the macro-morphological observations and zones of carbonate accumulation.

The carbonate content of both, the matrix and coating samples, varied between 21.0% and 40.9% with the lowest values in the middle part and higher values in the upper and lower parts (Figure 4C). The carbonate content of coatings was generally higher than the matrix samples (Figure 4C).

4.3 Radiocarbon dating and chronological model

The results of the radiocarbon chronology of carbonate coatings and the age-depth model are presented in Table 2; Figure 5, respectively. The radiocarbon ages strongly increased with depth within the first 40 cm, followed by a small age inversion at about 50 cm and then, again, a strong age increase in age down to about 80 cm soil depth. The lower part of the

soil (at about 80–150 cm depth) is characterised by a much smaller age increase where a maximum age of about 32 ka BP is finally reached. These ages represent mostly the real-time conditions. If old soil organic matter is respired, then the produced CO₂ may influence the age of secondary carbonates (Wang et al., 1994). In such a case, the radiocarbon ages correspond to a maximum age. Due to the fact that the investigated soil contains only very little org. C, the likelihood is relatively high that the radiocarbon ages predominantly indicate the formation of secondary carbonates that are formed from dissolved atmospheric and root respiration derived CO₂ in the soil percolation water.

4.4 Stable isotope geochemistry of pedogenic carbonates

The stable oxygen and carbon isotope composition of the studied carbonates is given in Tables 3, 4, respectively. The δ¹³C

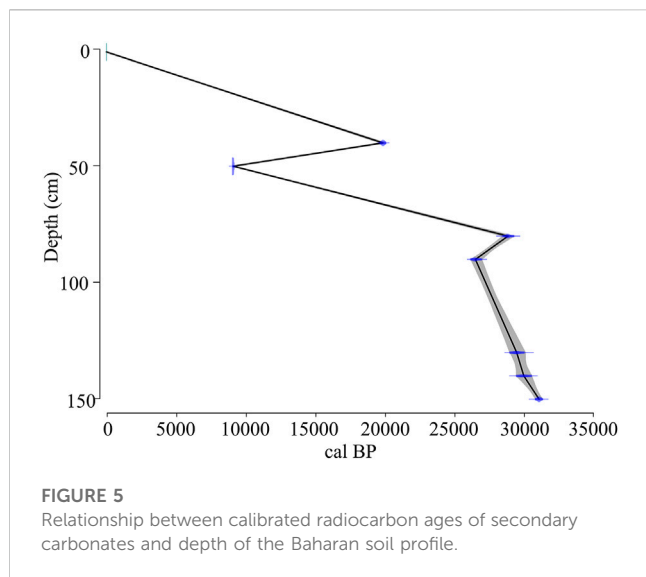


FIGURE 5
Relationship between calibrated radiocarbon ages of secondary carbonates and depth of the Baharan soil profile.

values of the bulk soil samples and coating carbonates are presented in Table 4; Figure 6A. The almost identical trend of the $\delta^{13}\text{C}$ values in the bulk soil and the matrix carbonates indicates the major role of carbonates in determining the $\delta^{13}\text{C}$ values of the bulk soil—also due to the low OC content (Figure 6A; Table 1). The trend of the C isotope values of the matrix carbonates with depth can be divided into three parts: in an uppermost part (0–20 cm) where the $\delta^{13}\text{C}$

ratio is highest. The second part is at a depth of 40–60 cm and indicates moderately low $\delta^{13}\text{C}$ values. The third part is from 60 to ~160 cm with relatively constant $\delta^{13}\text{C}$ values (Figure 6A).

The $\delta^{18}\text{O}$ -depth relationship of the investigated carbonates and—for comparison—the Gharneh palaeosols are presented in Figure 6B. The graph shows a gradual increase in the $\delta^{18}\text{O}$ value of the matrix carbonates towards the soil surface where it reaches its maximum in the vesicular horizon. The $\delta^{18}\text{O}$ values of the coating carbonates are similar to the matrix with some relative enrichment. The $\delta^{18}\text{O}$ values varied between -8.5 and -3.9‰ with a mean of -7.5‰ for matrix carbonates and -8.5 to -6.1‰ for coatings having a mean of -7.3‰ (Table 3). The carbon isotopic values are in the range of -3.4 and $+0.7$ and -3.7 to -1.3‰ for the matrix and coating carbonates, respectively (Table 4). Generally, the matrix carbonates had slightly lower average $\delta^{18}\text{O}$ values and higher $\delta^{13}\text{C}$ values compared to the carbonate coatings.

5 Discussion

5.1 Leaching and calcification of the baharan palaeosol

The abundance of coarse and well-rounded gravel and pebbles in the profile (Figure 2) suggest that the original sediment was likely transported and deposited by a high-energy medium (Shlemon, 1978) such as a palaeo-deltaic environment associated with the

TABLE 3 Stable oxygen isotopic values for the studied carbonates.

Depth	Age (a BP) ^a	$\delta^{18}\text{O}$	
		(carbonate of soil matrix, ‰)	(secondary carbonate, ‰)
0–4	232	-3.9	n.d.
4–14	1,203	-6.2	n.d.
14–24	3,963	-6.9	n.d.
24–34	7,754	-6.9	n.d.
34–44	12026	-7.3	-7.5
44–54	16323	-7.7	-6.2
54–64	20290	-7.9	n.d.
64–74	23673	-7.9	n.d.
74–84	26313	-8.5	-6.1
84–94	28153	-8.3	-8.5
94–104	29235	-7.5	n.d.
104–114	29700	-7.5	n.d.
114–124	29787	-8.3	n.d.
124–134	29835	-8.4	-7.2
134–144	30282	-8.2	-8.0
144–154	31665	-8.3	-8.0
Average	-	-7.5	-7.3

^aAges from ^{14}C age-depth trend; n.d. = not determined.

TABLE 4 Stable carbon isotopic values for the studied carbonates and paleoenvironmental interpretations.

Depth	Age	$\delta^{13}\text{C}$	$\delta^{13}\text{C}$	$\Delta^{13}\text{C}^2$	$\delta^{13}\text{C}$	$\Delta^{13}\text{C}$	% C4	% C3	Atmospheric	$\delta^{13}\text{C}$	Atmospheric
	(a BP) ^a	(Bulk soil, ‰)	(Matrix carbonate, ‰)	(Matrix carbonate, ‰)	(Rind carbonate, ‰)	(Rind carbonate, ‰)			CO ₂ (ppmv) ³	Atmospheric CO ₂ (‰) ⁴	CO ₂ Incorporation (%)
0–4	232	0.25	0.69	23.19	n.d.	n.d.	n.d.	n.d.	275	–6.50	n. d.
4–14	1,203	–1.52	–0.83	21.67	n.d.	n.d.	n.d.	n.d.	278	–6.43	44.1
14–24	3,963	–2.57	–1.90	20.6	n.d.	n.d.	n.d.	n.d.	271	–6.33	37.3
24–34	7,754	–2.43	–1.90	20.6	n.d.	n.d.	n.d.	n.d.	261	–6.35	37.3
34–44	12026	–2.36	–1.78	20.72	–1.53	20.97	n.d.	n.d.	257	–6.70	36.8
44–54	16323	–2.87	–2.10	20.4	–1.32	21.18	n.d.	n.d.	212	–6.69	30.5
54–64	20290	–3.73	–3.02	19.48	n.d.	n.d.	n.d.	n.d.	194	–6.45	n.d.
64–74	23673	–3.94	–3.17	19.33	n.d.	n.d.	n.d.	n.d.	196	–6.45	n.d.
74–84	26313	–3.44	–3.16	19.34	–3.69	18.81	70.96	29.04	196	–6.39	n.d.
84–94	28153	–4.23	–3.36	19.14	–2.91	19.59	69.55	30.45	196	–6.39	n.d.
94–104	29235	–4.27	–3.14	19.36	n.d.	n.d.	71.16	28.84	199	–6.40	n.d.
104–114	29700	–3.98	–3.08	19.42	n.d.	n.d.	71.55	28.45	198	–6.40	n.d.
114–124	29787	–3.55	–2.76	19.74	n.d.	n.d.	73.89	26.11	198	–6.40	n.d.
124–134	29835	–3.72	–2.90	19.6	–3.03	19.47	72.88	27.12	197	–6.40	n.d.
134–144	30282	–3.75	–3.03	19.47	–2.71	19.79	71.89	28.11	194	–6.41	n.d.
144–154	31665	–3.60	–3.14	19.36	–3.65	18.85	71.11	28.89	195	–6.42	n.d.
Mean	-	–3.10	–2.41	-	–2.69	-	71.59	28.41	-	-	-

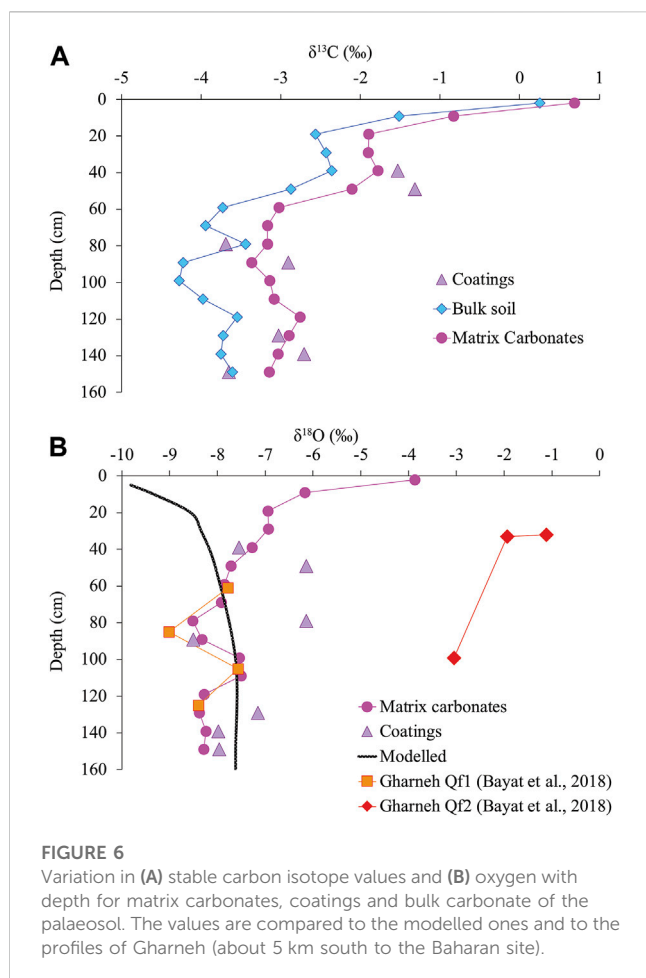
^aAges from ¹⁴C age-depth trend.

^b $\Delta^{13}\text{C} = \delta^{13}\text{C}_{\text{Measured}} - \delta^{13}\text{C}_{\text{SOM}}$, where $\delta^{13}\text{C}_{\text{SOM}} = -22.50\text{‰}$ (PDB).

^cAtmospheric CO₂ concentration for the Lateglacial (from the WAIS, Divide ice core; [Busaka et al., 2021](#)) and the Holocene (from Taylor Dome; [Monnin et al., 2004](#)).

^dAtmospheric isotopic values from Antarctica ice cores (from [Eggelston et al., 2016](#)).

nd. not determined.



Gavkhoni palaeo-lake (Bayat, 2007; Ghaiumi Mohammadi, 2011). The abundant and large gravels are resistant to deflation, wind and water erosion (Poesen and Lavee, 1994; Novák and Hlaváčiková, 2019).

The geochemical indices of leaching and calcification showed that the Baharan soil profile experienced several episodes of leaching and carbonate accumulation. Carbonate coatings formed through a progressive accumulation of thin rinds of carbonates (Machette, 1985; Pustovoytov, 2003; Zamanian et al., 2016), thus, the highest leaching index values and the highest carbonate content of coatings near the soil surface (both at a depth ~40 cm) imply repeated episodes of carbonate leaching and deposition in the upper part of the profile. The carbonate content of the coatings at greater depths was similar to those of the soil matrix (Figure 4C) suggesting restricted episodes of deep leaching and a reduction of the depth of leaching and rainfall during pedogenesis. This interpretation is supported by the accumulation of gypsum crystals on the surface of carbonate coatings. Consequently, the gypsum deposits must be younger than the carbonate precipitation. Gypsum occurs in layers where the carbonates have a maximum age of about 10–16 kyr. Therefore, gypsum indicates evaporite conditions (Kong et al., 2022) for at least part of the Holocene and probably the Late Pleistocene.

5.2 Stable isotope geochemistry of pedogenic carbonates

5.2.1. Stable oxygen isotopes

The $\delta^{18}\text{O}$ values of soil carbonates depend on the $\delta^{18}\text{O}$ values of the soil water and the temperature of the crystallisation (Cerling, 1984; Cerling and Quade, 1993; Quade, 2014). The $\delta^{18}\text{O}$ value of soil water is controlled by meteoric water which is a function of the latitude, the amount and source of rainfall, seasonality, mean annual temperature and follows the Rayleigh distillation model (i.e., fractionation of oxygen isotopes during evaporation-condensation processes) (Rozanski et al., 1992; Gat, 1996; Hsieh et al., 1998; Hoefs, 2021). It furthermore depends on changes in the soil environment. The movement of water in soil pores or its uptake by plant roots does not affect oxygen isotope composition of the soil water (Gat, 1996) but evaporation can increase the $\delta^{18}\text{O}$ value of soil water up to +7‰ (Hsieh et al., 1998) or even +10‰ (Gat, 1996). The evaporation enrichment is linearly related to the relative humidity in the local ecosystem (Quade, 2014) and was discussed for the deserts of Mojave (Amundson et al., 1989), Thar (Andrews et al., 1998; Achyuthan et al., 2007), Chihahuan (Monger et al., 1998), Atacama (Ebeling et al., 2016; Oerter et al., 2016) and central Iran (Bayat et al., 2018).

The shape of the $\delta^{18}\text{O}$ -depth trend for the matrix carbonates (Figure 6B) is similar to the shape of the $\delta^{18}\text{O}$ profile of soil water (especially in the upper parts) presented by Barnes and Allison (1983) for evaporation-affected soils suggesting the dominant role of evaporation on the oxygen isotope composition of the studied carbonates.

In order to evaluate and highlight the role of evaporation on the enrichment of oxygen isotopic values of the carbonates, we modelled the $\delta^{18}\text{O}$ values of pedogenic carbonates under the present climatic conditions. In general, authigenic calcite in soils forms slowly through the production of bicarbonate and Ca ions and subsequent crystallisation. The deposition of secondary calcite is promoted by a decrease in soil pCO_2 (lower biological activities and soil respiration rates), an increase in the rates of evaporation and soil temperature (warm and dry conditions) (Dever et al., 1987; Zamanian et al., 2016). A seasonal bias in precipitation of calcite in soils can be revealed by the isotope composition of modern soils (Amundson et al., 1989; Breecker et al., 2009; Khormali et al., 2020), thermodynamic modelling (Domínguez-Villar et al., 2022) and the clumped geothermometry of carbonates (Kelson et al., 2020). Pedogenic carbonate formation takes place during the warm and dry parts of the year. Here, we assume that the production of bicarbonate ions occurs during the wet season (February–May when ~55% of MAP occurs) followed by a subsequent crystallisation in the warm and dry months (June–August when the maximum temperatures are reached and only ~3% of MAP occurs; see also Khormali et al., 2020). Modelling was done using the fractionation factor of Kim and O'Neil (1997). Furthermore, the $\delta^{18}\text{O}$ values of local meteoric water for the months February–May and soil temperatures at different depths at the Kaboutarabad meteorological station during June–August were used for modelling. This model predicts the $\delta^{18}\text{O}$ values of carbonates at different depths under the present temperature and rainfall regime and without any evaporative enrichment (Figure 6B).

The modelling results showed an exponential increase in the $\delta^{18}\text{O}$ values with depth reaching constant values at a depth of c. 100 cm. The comparison of measured and modelled oxygen isotope values indicates that the $\delta^{18}\text{O}$ values of both matrix and coating carbonates in the upper 60 cm (especially in the upper 20 cm) of the pedon are enriched ($\sim 4\%$) relative to the predicted values which is mainly related to the impact of evaporation (Figure 6B). Moreover, because the highest oxygen isotopic values are recorded in the vesicular horizon (Table 3), the input of fine-grained primary calcite by calcareous dust could have affected the $\delta^{18}\text{O}$ values of the matrix carbonates in the topsoil.

The matrix carbonates in the deeper parts have generally lower isotopic values compared to the model suggesting their formation under different climatic conditions (higher precipitation and/or lower temperatures). The deep leaching of these carbonates supports the assumption that their deposition occurred in response to higher precipitation.

To further investigate the oxygen isotope composition of carbonates in the Baharan palaeosol, the data was compared to the nearby Gharneh palaeosols that showed two distinct trends. At Gharneh, carbonates of the younger geomorphic surface (Qf2) were in the first stages of development (Bayat et al., 2018) and had high $\delta^{18}\text{O}$ values which shows that they were formed under the present arid and evaporative environmental conditions (Figure 6B). The powdery morphology of these carbonates supports this hypothesis. The great depth of these carbonates is likely due to the penetration of water from the runoff of the alluvial fan environment. In contrast, the carbonates of the older geomorphic surface at Gharneh (Qf1) having a more developed morphology (stages III and IV) are surprisingly in close agreement with the values of the matrix carbonates of the Baharan palaeosol suggesting that their formation occurred under similar environmental conditions (Figure 6B).

Overall, the oxygen isotopic record of the Baharan soil profile showed two distinct parts interpreted as evaporative-enriched (in the surface up to 60 cm) and depleted (60–160 cm) phases likely mirroring the hydrological changes in central Iran during the late Quaternary.

5.2.2. Stable carbon isotopes

The $\delta^{13}\text{C}$ record of soil carbonates is an indicator of carbon dynamics and turnover in soils of arid and semi-arid regions (Sheldon and Tabor, 2009). The carbon isotopic composition of soil carbonate is directly related to the $\delta^{13}\text{C}$ values of soil respiration and atmospheric CO_2 influx (Cerling, 1984; Cerling and Quade, 1993; Quade, 2014) and is indirectly controlled by environmental aridity and climatic parameters (Amundson et al., 1989; Bayat et al., 2021). Based on the C and O isotopes, Achyuthan et al. (2007) were able to reconstruct major changes in vegetation (C3 vs. C4 plants) using pedogenic carbonates over the last about 250 kyr.

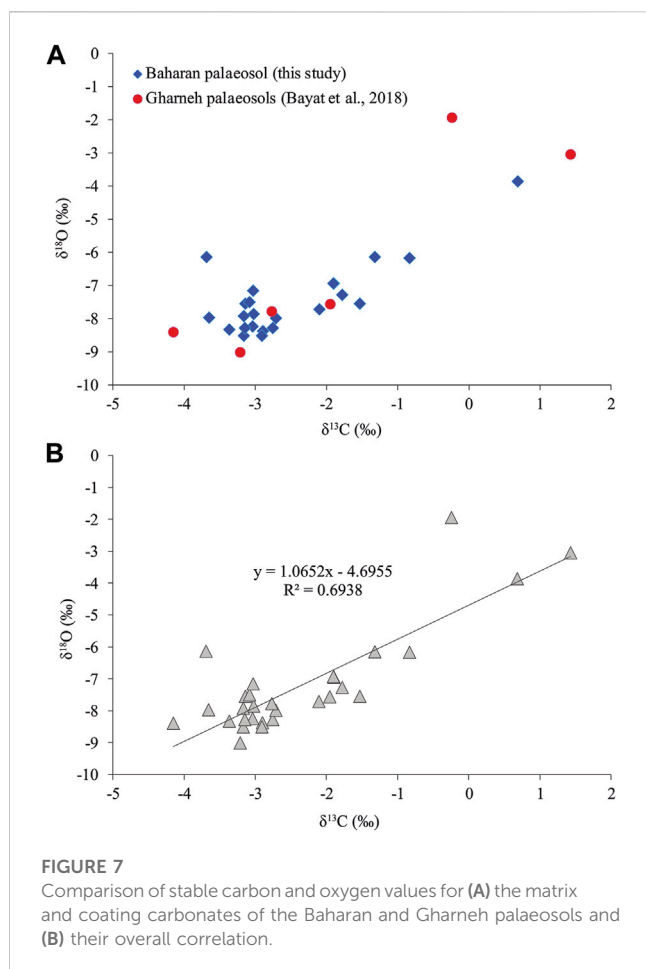
Generally, the $\delta^{13}\text{C}$ value of pedogenic carbonate ($\delta^{13}\text{C}_{\text{PC}}$) is a function of the $\delta^{13}\text{C}$ value of soil CO_2 ($\delta^{13}\text{C}_{\text{SC}}$) and the enrichment due to a diffusion fractionation ($\epsilon_{\text{CO}_2 \text{ diffusion fractionation}}$) and equilibrium fractionation ($\epsilon_{\text{CO}_2\text{-CaCO}_3}$) (Cerling, 1984; Romanek et al., 1992):

$$\delta^{13}\text{C}_{\text{PC}} = \delta^{13}\text{C}_{\text{SC}} + \epsilon_{\text{CO}_2 \text{ diffusion fractionation}} + \epsilon_{\text{CO}_2\text{-CaCO}_3} \quad (5)$$

The $\delta^{13}\text{C}$ values of the soil- CO_2 ($\delta^{13}\text{C}_{\text{SC}}$) depend on (1) the soil respiration rate and oxidation of the *in situ* organic matter controlled by the relative biomass contribution of plants (C₃, C₄, CAM) to soil organic matter pools. C₃ plants have a $\delta^{13}\text{C}$ signal of about -27% for a pure community while C₄ plants are near -13% (Ehleringer and Cerling, 2001; Ehleringer and Cerling, 2002). CAM plants consist mainly of desert succulents having $\delta^{13}\text{C}$ ratios between C₃ and C₄ plants (Ehleringer and Cerling, 2001; Ehleringer and Cerling, 2002). Soil- CO_2 production (respiration) influences the diffusion rate of atmospheric CO_2 into the soil. (2) The dissolution of primary carbonates or silicates and (3) the influx of atmospheric CO_2 also determines the $\delta^{13}\text{C}$ signal. The $\delta^{13}\text{C}$ values of modern and pre-industrial (ca. 1850) atmospheric CO_2 are approximately -8% and -6.5% , respectively (Cerling and Quade, 1993), which is significantly higher than the $\delta^{13}\text{C}$ values produced by higher plants (-27% , -13%). Thus, soils having a low vegetation cover have a greater atmospheric influx and mixing, especially in the upper parts than soils with a high rate of CO_2 production (Amundson et al., 1989; Pendall et al., 1994; Ebeling et al., 2016). The $\epsilon_{\text{CO}_2 \text{ diffusion fractionation}}$ describes the faster diffusion of the lighter $^{12}\text{CO}_2$ molecules out of the soil giving rise to a 4.4% increase in the $\delta^{13}\text{C}$ values of soil- CO_2 compared to soil-respired CO_2 from plant roots and the decomposition of organic material (Cerling, 1984; Cerling and Quade, 1993). Because of physical differences, the heavier ^{13}C isotope is preferentially retained in the solid phase during calcite precipitation (Romanek et al., 1992; Cerling and Quade, 1993).

Considering a soil temperature of 28.4°C (average soil temperature between June–August for depths 5 to about 50 cm (Supplementary Figure S3)) for the study area, the $\delta^{13}\text{C}$ values of soil carbonates would be enriched by about 13.0% compared to the corresponding soil- CO_2 and organic matter. If the difference between the $\delta^{13}\text{C}$ values of soil carbonate and the $\delta^{13}\text{C}$ values of soil organic matter ($\Delta^{13}\text{C} = \delta^{13}\text{C}_{\text{PC}} - \delta^{13}\text{C}_{\text{SOM}}$) is larger than this value, the carbonates are not in an isotopic equilibrium with soil organic matter (current vegetation cover) and are influenced by other environmental parameters. The results showed that all of the examined carbonates had $\Delta^{13}\text{C}$ values significantly higher than 13.0% and varied between 19.1% and 23.2% in the matrix carbonates and 18.8% – 21.2% in the coating carbonates (Table 4). Therefore, all studied carbonates are in isotopic disequilibrium with the modern vegetation cover of the study area and are enriched to different degrees.

Regarding the responsible factors determining the $\delta^{13}\text{C}$ values of pedogenic carbonates, several potential causes may be responsible for the disequilibrium between soil carbonates and modern vegetation: (1) contamination of soil carbonates with inherited calcareous material, especially marine limestone (Amundson et al., 1989; Khademi and Mermut, 1999), (2) diagenetic alteration of the pedogenic carbonates by post-depositional processes (Budd et al., 2002), (3) diffusion of atmospheric gas having high $\delta^{13}\text{C}$ values into the soil due to a low vegetation cover and low respiration rates (Amundson et al., 1989; Pendall et al., 1994; Monger et al., 1998; Ebeling et al., 2016; Bayat et al., 2018) and (4) changes in the proportion of C₃/C₄ plants in the local ecosystem (Cerling, 1984; Cerling and Quade, 1993; Andrews et al., 1998; Monger et al., 1998; Achyuthan et al., 2007; Railsback, 2021;



Sarangí et al., 2021; Fernández et al., 2022). Since the carbonates of the Baharan palaeosol are developed on non-calcareous clasts and are in the early stages of development, we can exclude causes 1 and 2. Thus, we will explore the impact of environmental factors (palaeoecological changes and the influx of atmospheric CO_2 into the soil) on the carbon isotope composition of the carbonates.

Previous studies revealed that the input of atmospheric CO_2 can influence the isotopic composition of shallow carbonates (Pendall et al., 1994; Budd et al., 2002). The shape of the $\delta^{13}\text{C}$ ratios along the profile for both bulk and matrix samples strongly suggest the input of heavy carbon isotopes in the upper 60 cm. Hence, we calculated the contribution of atmospheric CO_2 input on the C isotopes of the carbonates using a mass balance model (Eq. 2) and the $\delta^{13}\text{C}$ values of atmospheric CO_2 from Antarctic ice cores from Eggleston et al. (2016). The results indicated that the contribution of atmospheric CO_2 in the carbonate formation increased from around 30% at depth ~50 cm to roughly 44% in the near-surface carbonates (Table 4). Furthermore, the vesicular (dust accumulated) horizon in the uppermost part of the profile contained the highest $\delta^{13}\text{C}$ value (Figure 6A). Since limestone rocks with high $\delta^{13}\text{C}$ values ($\delta^{13}\text{C}$: +2.6 to +3.4‰, Khademi and Mermut, 1999) and limestone derived soils are present in the study area (Khademi and Mermut, 1999; Bayat et al., 2017; Bayat et al., 2018), it seems that dust input having a heavy isotope composition probably also influenced the topsoil of the Baharan

profile. Unfortunately, there is no data on the isotopic composition of modern dust and the late Quaternary history of aeolian processes in the region, but we can conclude that the combination of both atmospheric CO_2 and calcareous dust-controlled carbon isotope sources are recorded in the upper horizons of the profile.

We examined the relationship between the isotope composition of carbonates in the Baharan palaeosol and palaeosols of adjacent landforms (Gharneh alluvial fan, Figure 7). The isotope values and correlation between $\delta^{18}\text{O}$ and $\delta^{13}\text{C}$ values for the matrix and rind carbonates in the Baharan palaeosol and Gharneh palaeosols showed a positive correlation (Figure 7). Since carbonate coatings are certainly of pedogenic origin (Pendall et al., 1994; Amundson et al., 1997; Oerter et al., 2016), the strong correlation to the matrix carbonates also demonstrates a pedogenic origin of matrix carbonates.

It seems that palaeoecological changes influenced the C isotope composition of carbonates at greater depths because they were formed under a sub-humid climate (higher palaeoprecipitation values), higher vegetation density and soil respiration rates. Moreover, atmospheric CO_2 cannot penetrate into deep depths of soils (Pendall et al., 1994; Budd et al., 2002). Changes in the vegetation cover are controlled by environmental and climatic factors such as temperature, effective moisture and atmospheric CO_2 partial pressure (Ehleringer and Cerling, 2001; Ehleringer and Cerling, 2002). The calculated values for ecological conditions during carbonate formation imply an expansion of C_4 plants during their formation (mean C_4 = 71.6%, C_3 = 28.4%, Table 4). This palaeoecological condition stands in contrast to the present-day situation with 63% of C_3 native plants (Khademi and Mermut, 1999). As the photosynthetic efficiency of C_4 plants favours their expansion at low levels of atmospheric CO_2 concentrations (Ehleringer and Cerling, 2001; Ehleringer and Cerling, 2002), we can relate the expansion of these plants in the study area to the impact of global change of atmospheric CO_2 concentration. This interpretation is in good agreement with the expansion of C_4 plants during the late Quaternary as a response to low atmospheric CO_2 levels in the Chihahuan Desert of New Mexico (Monger et al., 1998) and the Thar Desert of India (Andrews et al., 1998; Achyuthan et al., 2007).

5.3 Environmental dynamics in the eastern isfahan, central Iran, over the last 32 ka

Generally, the ages of carbonate coatings increased with depth to about 32 kyr. The values of radiocarbon dates of carbonates depend on the $^{14}\text{C}/^{12}\text{C}$ ratio in the atmosphere during the initial stage of carbonate formation and post-depositional contamination with environmental ^{14}C values (Amundson et al., 1994; Pendall et al., 1994; Pustovoytov, 1998; Pustovoytov, 2003; Dal Sasso et al., 2018). Contamination of carbonates by primary carbonates (e.g., marine limestone) or CO_2 gas from decomposition of old organic materials can result in an overestimation of the ages (Amundson et al., 1989; Pustovoytov, 2003). In contrast, recrystallisation processes, diagenetic alteration, re-equilibrium and incorporation of younger ^{14}C (e.g., by shallow ground water) may cause an

underestimation of the age (Geyh and Eitel, 1998; Budd et al., 2002; Zamanian et al., 2016). Carbonate coatings in gravelly soils, especially in the early stages of development, are of major interest for a radiocarbon chronology because of their pedogenic origin, minor contamination by detrital material (Amundson et al., 1989; Amundson et al., 1994) and also the time-dependent nature of rinds (Machette, 1985; Pustovoytov, 2003). Because the carbonates of the Baharan soil profile formed in non-calcareous gravels, they were neither contaminated by primary marine carbonates nor by groundwater (Amundson et al., 1989; Amundson et al., 1994; Geyh and Eitel, 1998). Moreover, these carbonates formed in the early stages of soil development and are not influenced by diagenetic alterations. Thus, these carbonates reflect a reliable situation. Our results reveal that pedogenic carbonates formed during the last 32 ka with periods of intense calcification between 32 and 26 ka (Table 2; Figure 5).

To reconstruct palaeoprecipitation from pedogenic carbonates, the following points must be fulfilled., (Retallack, 2005): (i) the soil carbonates must be of pedogenic origin and in the early-middle stages of development (nodules) having a micritic microstructure, (ii) the soil must have developed in unconsolidated materials (alluvium, loess) and has not been affected by erosion or burial processes and (iii) the carbonates did not form during geological periods of elevated atmospheric CO₂ concentrations and impacts of acidic rain (Retallack, 1994; Retallack, 2005; Sheldon and Tabor, 2009; Beverly et al., 2018). The carbonates of the Baharan profile exhibited coatings and nodules (stage II of development) and are developed in coarse-grained alluvium having free-drainage conditions and there are no indications of burial. The coarse grains of the palaeosol are very resistant to erosion by both wind and water. Moreover, the palaeosol has a flat surface that minimises the lateral movement of water on the landform. Hence, the Baharan palaeosol is quite suitable for the reconstruction of palaeoprecipitation. The results of the estimation using the depth of nodules associated with coatings are presented in Figure 8. Variations in palaeoprecipitation and leaching depths could be traced for the last 32 kyr. It seems that three main stages of palaeoenvironmental changes occurred in the region as recorded in the oxygen and carbon isotope composition of pedogenic carbonates (Figure 9). The first stage was accompanied by deep leaching under sub-humid (MAP ~700 mm), seasonal climatic conditions and the expansion of C₄ plants. This phase lasted ca. 5,000 years (31.6 and 26.0 ka) which corresponds to the MIS3/2 transitional stage and exhibited humid to sub-humid conditions with MAP of around 500–700 mm. These MAP values correspond to strong decalcification of soils in the Mediterranean regions (Yaalon, 1997). The investigation of n-alkane proxies in a loess/palaeosol profile in arid central Asia revealed warm and humid condition during the MIS3/2 stages and a change to drier condition during MIS 2 (Yang and Jing, 2022). The second phase (~26.0–3.0 ka) was accompanied by a gradual increase in the δ¹⁸O values and aridity in the region and a dominance of a semi-arid (MAP ~375 mm) climate during MIS 2 until the late Holocene. The last phase reflects an arid and chiefly evaporative environment with sparse vegetation cover and dust influx (Figure 9).

Since the last glacial maximum (LGM, ~20 ka), aridification is recorded both in the δ¹⁸O and δ¹³C values of the carbonates (Figure 9; see, e.g.; Achyuthan et al., 2007). C₃ plants growing in arid environments tend to have more positive δ¹³C values compared to those growing under less water-stressed conditions (Ehleringer, 1988). This aridity was intensified during the late Holocene. We assume that an increase in evaporation and the decline of the vegetation cover as well as the input of dust into the soil were responsible for the high isotopic values in the top soil. The aridity, cold and windy conditions resulted in loess deposition and sand ramp formation in north-eastern and central Iran, respectively (Thomas et al., 1997; Karimi et al., 2011) and are also recorded in the fluvial deposits of the Kalshur River system in north-eastern Iran (Khosravichenar et al., 2020). Moreover, stable isotopic composition of stalagmites in the southern part of the Zagros mountains revealed cold and dry conditions in the region during the LGM (Soleimani et al., 2023). It seems that windy, cold and dry conditions during the LGM were a consequence of the dominance of the Siberian High over the region (Thomas et al., 1997). Simulations of the LGM dust cycle using a climate-dust model showed that cool, dry and eastern winds, produced by a high-pressure over the Eurasian ice sheet, were dominant in Europe during LGM resulting in loess depositions in eastern and central Europe (Schaffernicht et al., 2020).

To better understand the nature and dynamics of regional climatic changes during the late Quaternary, the δ¹⁸O values and climatic stages of the study area were compared with δ¹⁸O values of secondary carbonates (speleothems) of the Soreq Cave in the eastern Mediterranean (Orland et al., 2012) and the Hoti Cave in northern Oman (Fleitmann et al., 2022) (Figure 10). The Soreq Cave is located 40 km inland from the Mediterranean Sea having a semi-arid climate (MAP ~500 mm) that is dominated by winter precipitation (Bar-Matthews et al., 1999; Orland et al., 2012). This site represents the activity of the Mediterranean cyclones in the western Asia while the Hoti Cave, located in a monsoon-dominated region with summer rainfalls (MAP ~150 mm), is an indicator of changes in summer monsoon activities in the western Asia (Fleitmann et al., 2022). Generally, the controlling factors on the oxygen isotope composition of the cave water and speleothems are similar to those of the soil carbonates and depend on mean annual temperature, rainfall source and amount and evaporation rates (Bar-Matthews et al., 1999). The comparison showed that the δ¹⁸O values trends of central Iran and the eastern Mediterranean are identical between ~32 and 26 ka suggesting similar climatic mechanisms of the regions while the Hoti Cave represented an inverse trend during this period. Based on our carbon isotopic data, this period was accompanied by the expansion of C₄ plants in eastern Isfahan under a semi-arid climate. The second phase (26.0–3.0 ka BP) is characterised by a gradual increase in environmental aridity due to a reduction of rainfall or rise in temperatures or both in central Iran. During this interval, the δ¹⁸O values of the Soreq Cave declined significantly while the oxygen isotopes in the Hoti Cave fluctuated considerably with a significant increase during early to mid-Holocene. The decrease in the oxygen isotope composition in the Soreq Cave went along with higher levels of the Dead Sea during MIS 2 (Torfstein et al., 2013) and indicated a diverging climatic trend in the eastern Mediterranean and Central Iran.

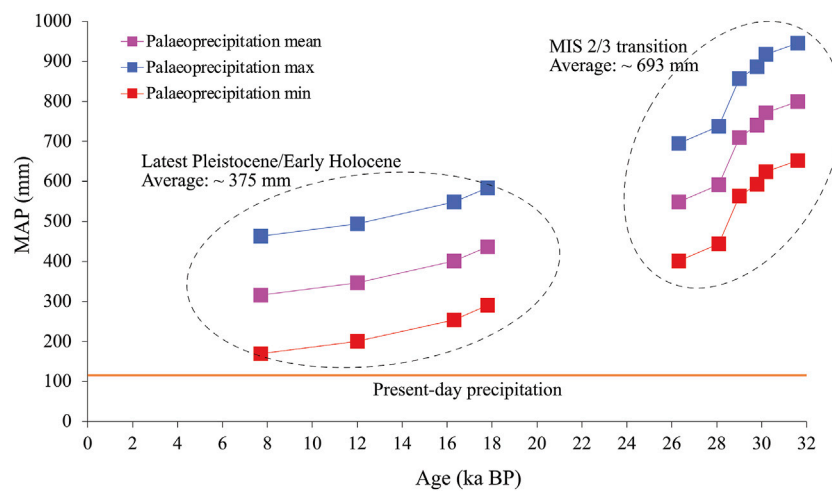


FIGURE 8
Palaeoprecipitation estimation for the marine isotope stage (MIS) 3/2 and the latest Pleistocene/early Holocene at Baharan.

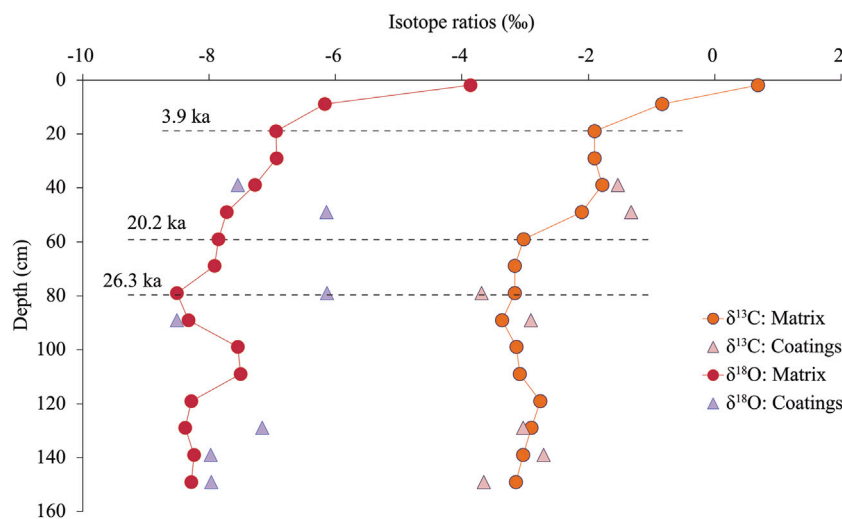


FIGURE 9
Depth functions of $\delta^{18}\text{O}$ and $\delta^{13}\text{C}$ values of the matrix and coating carbonates of the Baharan soil profile.

The increase in environmental aridity since the late Pleistocene is also recorded in the isotopic composition of bulk carbonates in the Mobarakabad Section, northern Iran (Ghafarpour et al., 2021). Other archives and proxies also exhibited a similar trend. Aubert et al. (2017) showed, by using pollen analysis, that the period between 15.5 and 12.7 kyr BP was relatively dry in northwest Iran. Based on a peat record, Sharifi et al. (2015) come to the conclusion that dusty and dry conditions prevail in northwest Iran since about 5 kyr which is consistent with orbital changes in insolation that affected much of the northern hemisphere. Since the Siberian high established over central Iran between 25–18 ka BP (Thomas et al., 1997), the penetration of Mediterranean cyclones into central Iran and the Middle East was most likely blocked by this anticyclone. The last

phase (3.0–0 ka BP) in both central Iran and northern Oman was accompanied by a marked increase in the $\delta^{18}\text{O}$ records owing to the dominance of aridity in the Middle East during the late Holocene. Although the eastern Mediterranean and northern Oman receive rainfall from different climatic systems, surprisingly, these regions have a relatively similar oxygen isotopic composition as shown in Supplementary Figure S1. The Mediterranean area has in general just a slightly lower $\delta^{18}\text{O}$ value. This is mainly because of the cool-season precipitation in the eastern Mediterranean (Orland et al., 2012) and the amount effect of the monsoonal rainfall in northern Oman (Hoefs, 2021). The reason why cave carbonates in northern Oman show higher isotopic values rather than in the eastern Mediterranean region (especially

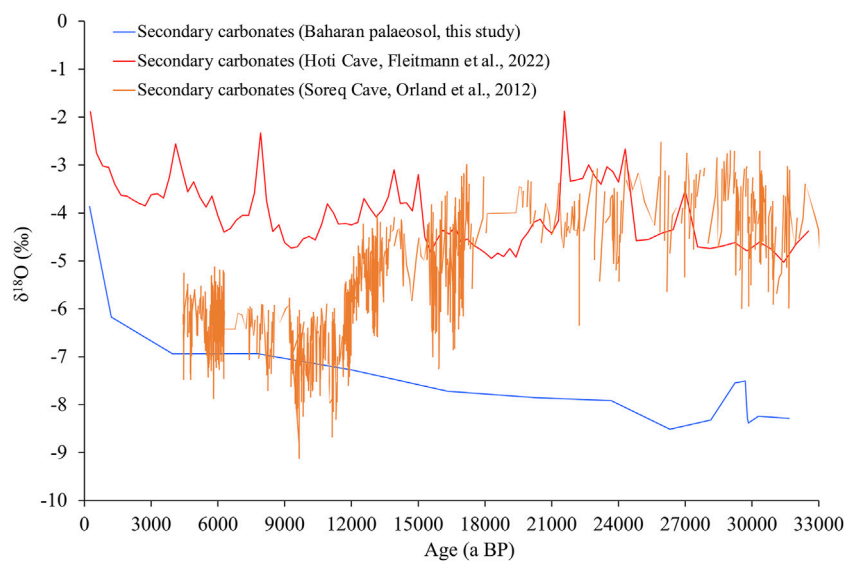


FIGURE 10

Variation of the $\delta^{18}\text{O}$ values of secondary carbonates in the Baharan palaeosol (this study), the Hoti Cave (northern Oman, after [Fleitmann et al., 2022](#)) and the Soreq Cave (eastern Mediterranean, after [Orland et al., 2012](#)) for the last 33000 years.

during the late Holocene) is the fact that meteoric water in this region was subjected to severe evaporation during the dry season and, thus, prior to calcite crystallization. Drought events in the Middle East during the late Holocene were also reflected in the isotopic record of the Gol-e-Zard Cave (NW Iran) and Gejkar Cave in northern Iraq ([Flohr et al., 2017](#); [Carolin et al., 2019](#)). This period is also reflected by high $\delta^{13}\text{C}$ values of the matrix carbonates due to the input of calcareous dust. This interpretation is supported by the measured high rates of dust input in the record of the Gol-e-Zard cave in NW Iran during the Late Holocene ([Carolin et al., 2019](#)).

6 Conclusion

Based on a high-resolution study of geochemical and stable isotope composition of soil carbonates (both matrix and coatings) in a relict palaeosol (Baharan soil profile), we conclude that.

- 1- The soil profile experienced several periods of leaching that were reflected in the morphology and geochemical characteristics.
- 2- The $\delta^{18}\text{O}$ values of both matrix and coating carbonates in the upper 60 cm (especially in the upper 20 cm) of the pedon are enriched ($\sim 4\%$) relative to the predicted values which is mainly related to the impact of evaporation. Moreover, the $\delta^{13}\text{C}$ values in all studied carbonates are in an isotope disequilibrium with the modern vegetation cover of the study area and are enriched in different degrees. The carbonates in the top 60 cm reflect the incorporation of atmospheric CO_2 and calcareous dust while the deeper carbonates formed in an environment having more C_4 plants.

3- It seems that three main stages of palaeoenvironmental changes have occurred in the region during the last 32 ka. The first stage (MIS3/2 transitional stage, 31.6–26.0 ka BP) was accompanied by deep leaching under sub-humid (MAP ~ 700 mm), seasonal climatic conditions and the expansion of C_4 plants. The second phase exhibited a gradual increase in the $\delta^{18}\text{O}$ values and aridity in the region. Semi-arid (MAP ~ 375 mm) conditions prevailed during MIS 2 until the late Holocene. The last phase is characterised by the establishment of an arid, evaporative environment with a very sparse vegetation cover and aeolian activity.

4- Aridification in central Iran started during the LGM and is recorded in both the $\delta^{18}\text{O}$ and $\delta^{13}\text{C}$ ratios of the studied carbonates. The aridity and aeolian activity even intensified during the late Holocene.

5- A regional climatic correlation based on the $\delta^{18}\text{O}$ composition of secondary carbonates of the Baharan palaeosol, the Soreq and Hoti caves revealed climatic connections between (i) central Iran and the eastern Mediterranean during the MIS 3/2 transition and (ii) central Iran and northern Oman during the late Holocene. It seems that the expansion of the Siberia High over central Iran ended at 25 ka BP the moist period of central Iran by blocking the penetration of Mediterranean storms.

7- Carbonate-bearing palaeosols, which are extensively distributed in arid and semi-arid landscapes, have a great potential to be a reliable proxy for deciphering a wide range of palaeoclimatic conditions.

Data availability statement

The original contributions presented in the study are included in the article/[Supplementary Material](#) further inquiries can be directed to the corresponding author.

Author contributions

OB, AK, and J-HM contributed to the conception and design of the research. OB and AK conducted the fieldwork and took the samples. ME and GW analysed the samples. OB wrote the first draft of the manuscript and ME revised it. ME, AK, and J-HM prepared the figures. ME, AK, and MF further discussed and corrected the manuscript. All authors contributed to the article and approved the submitted version.

Funding

This work was supported by a grant from the Ferdowsi University of Mashhad (grant no. 1/52230: 13/03/1399) and by the Swiss National Foundation (grant no. 200021_212055/1).

Acknowledgments

We thank Thomy Keller and Yves Brügger for their support in the laboratory. We are grateful for the comments of HA and DV-F on an earlier version of the manuscript.

References

- Achyuthan, H., Quade, J., Roe, L., and Placzek, C. (2007). Stable isotopic composition of pedogenic carbonates from the eastern margin of the Thar Desert, Rajasthan, India. *Quat. Int.* 162–163, 50–60. doi:10.1016/j.quaint.2006.10.031
- Amit, R., Enzel, Y., Grodek, T., Crouvi, O., Porat, N., and Ayalon, A. A. (2017). "Aridisols in the southern levant deserts and their palaeoclimate implications," in *Quaternary of the levant: Environments, climate change, and humans*. Editors Y. Enzel and O. Bar-Yosef (Cambridge: Cambridge University Press).
- Amundson, R., Chadwick, O., Sowers, J., and Doner, H. (1989). The stable isotope chemistry of pedogenic carbonates at Kyle Canyon, Nevada. *Soil Sci. Soc. Am. J.* 53, 201–210. doi:10.2136/sssaj1989.03615995005300010037x
- Amundson, R., Wang, Y., Chadwick, O., Trumbore, S., McFadden, L., McDonald, E., et al. (1994). Factors and processes governing the ^{14}C content of carbonate in desert soils. *Earth Planet. Sci. Lett.* 125, 385–405. doi:10.1016/0012-821x(94)90228-3
- Amundson, R., Graham, R. C., and Franco-Vizcaino, E. (1997). Orientation of carbonate laminations in gravelly soils along a winter-summer precipitation gradient in Baja California, Mexico. *Soil Sci.* 162, 940–952. doi:10.1097/00010694-199712000-00009
- Amundson, R. (2005). "Soil formation," in *Surface and groundwater, weathering and soils*. Editor J. I. Drever (Amsterdam: Elsevier), 1–35.
- Andrews, J. E., Singhvi, A. K., Kailath, A. J., Kuhn, R., Dennis, P. F., Tandon, S. K., et al. (1998). Do stable isotope data from calcrete record late Pleistocene monsoonal climate variation in the Thar Desert of India? *Quat. Res.* 50, 240–251. doi:10.1006/qres.1998.2002
- Aubert, C., Brisset, E., Djamali, M., Sharifi, A., Ponef, P., Gambin, B., et al. (2017). Late glacial and early Holocene hydroclimate variability in northwest Iran (Talesh Mountains) inferred from chironomid and pollen analysis. *J. Paleolimnol.* 58, 151–167. doi:10.1007/s10933-017-9969-8
- Bagheri, A. (2005). "Investigation of soil temperatures in the occurrence of frost phenomenon in the Kaboutarabad, Isfahan," in *Proceeding of the conference on cropping methods to frost* (Iran: Yazd), 121–125. (in Persian).
- Bar-Matthews, M., Ayalon, A., Kaufman, A., and Wasserburg, G. (1999). The Eastern Mediterranean paleoclimate as a reflection of regional events: Soreq cave, Israel. *Sci. Lett.* 166, 85–95. doi:10.1016/s0012-821x(98)00275-1
- Barnes, C. J., and Allison, G. B. (1983). The distribution of deuterium and ^{18}O in dry soils, 1. *Theory, J. hydro.* 60, 141–156. doi:10.1016/0022-1694(83)90018-5
- Bauska, T. K., Marcott, S. A., and Brook, E. J. (2021). Abrupt changes in the global carbon cycle during the last glacial period. *Nat. Geosci.* 14, 91–96. doi:10.1038/s41561-020-00680-2
- Bayat, O., Karimzadeh, H. R., Karimi, A., Eghbal, M. K., and Khademi, H. (2017). Paleoenvironment of geomorphic surfaces of an alluvial fan in the eastern Isfahan, Iran, in the light of micromorphology and clay mineralogy. *Arab. J. Geosci.* 10, 91. doi:10.1007/s12517-017-2848-9
- Bayat, O., Karimzadeh, H. R., Eghbal, M. K., Karimi, A., and Amundson, R. (2018). Calcic soils as indicators of profound Quaternary climate change in eastern Isfahan, Iran. *Geoderma* 315, 220–230. doi:10.1016/j.geoderma.2017.11.007
- Bayat, O., Karimi, A., and Amundson, R. (2021). "Stable isotope geochemistry of pedogenic carbonates in calcareous materials, Iran: A review and synthesis,". *Stable isotope studies of water cycle and terrestrial environments*. Editors A. Bojar, A. Pelc, and C. Lecuyer (London: Geological Society of London, Special Publication), 507, 255–272.
- Bayat, O. (2007). *Landscape evolution in eastern Isfahan based on stratigraphy and pedogenic evidence*. [Masters thesis]. Isfahan: Isfahan University of Technology.
- Beverly, E. J., Lukens, W. E., and Stinchcomb, G. E. (2018). "Paleopedology as a tool for reconstructing paleoenvironments and paleoecology," in *Methods in paleoecology*. Editors D. A. Croft, D. F. Su, and S. W. Simpson (Cham, Switzerland: Springer Nature), 151–183.
- Birkeland, P. W. (1999). *Soils and Geomorphology*. New York: Oxford University Press.
- Bowen, G. J. (2017). *The online isotopes in precipitation calculator, Version 3.1*. USA: University of Utah. Available at: <https://wateriso.utah.edu/waterisotopes/index.html>.
- Bradley, R. S. (2015). *Paleoclimatology: Reconstructing climates of the quaternary*. Amsterdam: Elsevier.
- Breecker, D. O., Sharp, Z. D., and McFadden, L. D. (2009). Seasonal bias in the formation and stable isotopic composition of pedogenic carbonate in modern soils from central New Mexico, USA. *Geol. Soc. Am. Bull.* 121 (3–4), 630–640. doi:10.1130/b26413.1
- Breitenbach, S. F., and Bernasconi, S. M. (2011). Carbon and oxygen isotope analysis of small carbonate samples (20 to 100 g) with a GasBench II preparation device. *Rapid Commun. Mass Spectrom.* 25 (13), 1910–1914. doi:10.1002/rcm.5052
- Bronk Ramsey, C. (2001). Development of the radiocarbon calibration program. *Radiocarbon* 43, 355–363. doi:10.1017/S0033822200038212
- Bronk Ramsey, C. (2009). Bayesian analysis of radiocarbon dates. *Radiocarbon* 51 (1), 337–360. doi:10.1017/s0033822200033865
- Budd, D. A., Pack, S. M., and Fogel, M. L. (2002). The destruction of paleoclimatic isotopic signals in Pleistocene carbonate soil nodules of Western Australia. *Palaeogeogr. Palaeoclimatol. Palaeoecol.* 188, 249–273. doi:10.1016/s0031-0182(02)00588-6
- Carolin, S. A., Walker, R. T., Day, C. C., Ersek, V., Sloan, R. A., Dee, M. W., et al. (2019). Precise timing of abrupt increase in dust activity in the Middle East coincident with 4.2 ka social change. *Proc. Nat. Acad. Sci. (PNAS)* 116 (1), 67–72. doi:10.1073/pnas.1808103115
- Cerling, T. E., and Quade, J. (1993). "Stable carbon and oxygen isotopes in soil carbonates,". *Climate change in continental isotopic records*. Editors P. K. Stewart, K. C. J. LohmannMcKenzie, and S. Savin (Washington, DC, WA: American Geophysical Union, Geophysical Monograph), 78, 217–231.

Conflict of interest

The authors declare that the research was conducted in the absence of any commercial or financial relationships that could be construed as a potential conflict of interest.

Publisher's note

All claims expressed in this article are solely those of the authors and do not necessarily represent those of their affiliated organizations, or those of the publisher, the editors and the reviewers. Any product that may be evaluated in this article, or claim that may be made by its manufacturer, is not guaranteed or endorsed by the publisher.

Supplementary material

The Supplementary Material for this article can be found online at: <https://www.frontiersin.org/articles/10.3389/feart.2023.1154544/full#supplementary-material>

- Cerling, T. E. (1984). The stable isotopic composition of modern soil carbonate and its relationship to climate. *Earth Planet. Sci. Lett.* 71, 229–240. doi:10.1016/0012-821x(84)90089-x
- Coplen, T. B., Brand, W. A., Gehre, M., Groning, M., Meijer, H. A., Toman, B., et al. (2006). New guidelines for $\delta^{13}\text{C}$ measurements. *Anal. Chem.* 78, 2439–2441. doi:10.1021/ac052027c
- Coplen, T. B. (1988). Normalization of oxygen and hydrogen isotope data. *Chem. Geol.* 72, 293–297. doi:10.1016/0168-9622(88)90042-5
- Dal Sasso, G., Zerboni, A., Maritan, L., Angelini, I., Compostella, C., Usai, D., et al. (2018). Radiocarbon dating reveals the timing of formation and development of pedogenic calcium carbonate concretions in central Sudan during the Holocene. *Geochim. Cosmochim. Acta* 238, 16–35. doi:10.1016/j.gca.2018.06.037
- Dever, L., Fonts, J. Ch., and Riché, G. (1987). Isotopic approach to calcite dissolution and precipitation in soils under semi-arid conditions. *Chem. Geol.* 66, 307–314. doi:10.1016/0168-9622(87)90050-9
- Dominguez-Villar, D., Bensa, A., N'vob, M., and Krklec, K. (2022). Causes and implications of the seasonal dissolution and precipitation of pedogenic carbonates in soils of karst regions — A thermodynamic model approach. *Geoderma* 423, 115962. doi:10.1016/j.geoderma.2022.115962
- Ebeling, A., Oerter, E., Valley, J. W., and Amundson, R. (2016). Relict soil evidence for profound quaternary aridification of the Atacama Desert, Chile. *Geoderma* 267, 196–206. doi:10.1016/j.geoderma.2015.12.010
- Eggleston, S., Schmitt, J., Bereiter, B., Schneider, R., and Fischer, H. (2016). Evolution of the stable carbon isotope composition of atmospheric CO_2 over the last glacial cycle. *Paleocean* 31, 434–452. doi:10.1002/2015pa002874
- Egli, M., and Fitze, P. (2001). Quantitative aspects of carbonate leaching of soils with differing ages and climates. *Catena* 46, 35–62. doi:10.1016/s0341-8162(01)00154-0
- Elheringer, J. R., and Cerling, T. E. (2001). "Photosynthetic pathways and climate," in *Global biogeochemical cycles in the climate system*. Editors E. D. Schulze, M. Heimann, S. P. Harrison, E. A. Holland, J. Lloyd, I. C. Prentice, et al. (San Diego: Academic Press), 267–277.
- Elheringer, J. R., and Cerling, T. E. (2002). "C3 and C4 photosynthesis," in *Encyclopedia of global environmental change*. Editors H. A. Mooney and J. Canadell (Chichester: John Wiley and Sons), 186–190.
- Elheringer, J. R. (1988). "Carbon isotope ratios arid physiological processes in arid and plants," in *Application of stable isotopic ratios to ecological research*. Editors P. W. Rundel, J. R. Elheringer, and K. A. Nagy (New York: Springer), 41–54.
- Fernández, D. V., Rebolledo, E. S., Sedov, S., and Pustovoytov, K. (2022). Provenance, and environment context of pedogenic carbonates formation from MIS 3 to MIS 1 in the Teotihuacan Valley, Mexico. *Quat. Int.* 618, 52–69. doi:10.1016/j.quaint.2021.03.019
- Fleitmann, D., Burns, S. J., Matter, A., Vheng, H., and Affolter, S. (2022). Moisture and seasonality shifts recorded in Holocene and Pleistocene speleothems from southeastern Arabia. *Geoph. Res. Lett.* 49, e2021GL097255. doi:10.1029/2021GL097255
- Flohr, P., Fleitmann, D., Zorita, E., Sadekov, A., Cheng, H., Bosomworth, M., et al. (2017). Late Holocene droughts in the Fertile Crescent recorded in a speleothem from northern Iraq. *Geoph. Res. Lett.* 44 (3), 1528–1536. doi:10.1002/2016gl071786
- Gat, J. R. (1996). Oxygen and hydrogen isotopes in the hydrological cycle. *Ann. Rev. Earth Planet. Sci.* 24, 225–262. doi:10.1146/annurev.earth.24.1.225
- Geyh, M. A., and Eitel, B. (1998). Radiometric dating of young and old calcrete. *Radiocarbon* 40 (2), 795–802. doi:10.1017/s0033822200018749
- Ghafarpour, A., Khorrami, F., Meng, X., Tazikeh, H., and Stevens, T. (2021). Late Pleistocene climate and dust source from the Mobarakabad loess-paleosol sequence, northern foothills of the Alborz Mountains, northern Iran. *Front. Earth. Sci.* 9, 795826. doi:10.3389/feart.2021.795826
- Ghaiumi Mohammadi, H. (2011). *The influence of morphogenic-pedogenic processes on natural and civil evolutions of the Zayandehroud at the Quaternary period*. [Dissertation]. Isfahan: University of Isfahan.
- Giorgi, F. (2006). Climate change hot-spots. *Geophy. Res. Lett.* 33, L08707. doi:10.1029/2006gl025734
- Gocke, M., Pustovoytov, K., Kuhn, P., Wiesenberg, G. L. B., Löscher, M., and Kuz'yakov, Y. (2011). Carbonate rhizoliths in loess and their implications for paleoenvironmental reconstruction revealed by isotopic composition: Delta C-13, $\delta^{13}\text{C}$. *Chem. Geol.* 283, 251–260. doi:10.1016/j.chemgeo.2011.01.022
- Gocke, M., Peth, S., and Wiesenberg, G. L. B. (2014). Lateral and depth variation of loess organic matter overprint related to rhizoliths — revealed by lipid molecular proxies and X-ray tomography. *Catena* 112, 72–85. doi:10.1016/j.catena.2012.11.011
- Goudie, A. S. (2013). *Arid and semi-arid Geomorphology*. Cambridge: Cambridge University Press.
- Hoefs, J. (2021). *Stable isotope geochemistry*. Cham: Springer.
- Hsieh, J. C. C., Chadwick, O. A., Kelly, E. F., and Savin, S. M. (1998). Oxygen isotopic composition of soil water: Quantifying evaporation and transpiration. *Geoderma* 82, 269–293. doi:10.1016/s0016-7061(97)00105-5
- Hua, Q., Barbetti, M., and Rakowski, A. Z. (2013). Atmospheric radiocarbon for the period 1950–2010. *Radiocarbon* 55, 2059–2072. doi:10.2458/azu_js_rc_v55i2.16177
- Jones, M. D., Abu-Jaber, N., AlShdaifat, A., Baird, D., Cook, B. I., Cuthbert, M. O., et al. (2019). 20,000 years of societal vulnerability and adaptation to climate change in Southwest Asia. *WIREs Water* 6 (2), e1330. doi:10.1002/wat2.1330
- Karimi, A., Frechen, M., Khademi, H., Kehl, M., and Jalalian, A. (2011). Chronostratigraphy of loess deposits in northeast Iran. *Quat. Int.* 234, 124–132. doi:10.1016/j.quaint.2009.08.002
- Kelson, J. R., Huntington, K. W., Breecker, D. O., Burgener, L. K., Gallagher, T. M., Hoke, G. D., et al. (2020). A proxy for all seasons? A synthesis of clumped isotope data from Holocene soil carbonates. *Quat. Sci. Rev.* 234, 106259. doi:10.1016/j.quascirev.2020.106259
- Khademi, H., and Mermut, A. R. (1999). Submicroscopy and stable isotope geochemistry of carbonates and associated polygorskite in Iranian Aridisols. *Euro. J. Soil Sci.* 50, 207–216. doi:10.1046/j.1365-2389.1999.t01-1-00237.x
- Khorrami, F., Shahriari, A., Ghafarpour, A., Kehl, M., Lehndorff, E., and Frechen, M. (2020). Pedogenic carbonates archive modern and past precipitation change – a transect study from soils and loess-paleosol sequences from northern Iran. *Quat. Int.* 552, 79–90. doi:10.1016/j.quaint.2019.12.011
- Khosravichenar, A., Fattahi, M., Amini, H., and von Suchodoletz, H. (2020). The potential of small mountain river systems for paleoenvironmental reconstructions in drylands—an example from the Binaloud Mountains in northeastern Iran. *Geosciences* 10, 448. doi:10.3390/geosciences10110448
- Kim, S.-T., and O'Neil, J. (1997). Equilibrium and nonequilibrium oxygen isotope effects in synthetic carbonates. *Geochim. Cosmochim. Acta* 61 (16), 3461–3475. doi:10.1016/s0016-7037(97)00169-5
- Kong, T., Tudryn, A., Gibert-Brunet, E., Tucholka, P., Motavalli-Anbaran, S.-H., Ahmady-Birgani, H., et al. (2022). 30,000 Years of the southwestern Lake Urmia (Iran) paleoenvironmental evolution inferred from mineralogical indicators from lake and watershed sediments. *J. Asian Earth Sci.* 239, 105387. doi:10.1016/j.jseaes.2022.105387
- Kutzbach, J. E., Chen, G., Cheng, H., Edwards, R. L., and Liu, Z. (2014). Potential role of winter rainfall in explaining increased moisture in the Mediterranean and Middle East during periods of maximum orbitally-forced insolation seasonality. *Clim. Dyn.* 42, 1079–1095. doi:10.1007/s00382-013-1692-1
- Machette, M. N. (1985). "Calcic soils of the southwestern United States," in *Soils and quaternary geology of the southwestern United States*. Editors D. I. Weide and M. L. Faber (Boulder, CO: Geological Society of America Special Paper 203), 1–21.
- Monger, H. C., Colegish, D. R. J. W., and Giordano, T. H. (1998). Stable carbon and oxygen isotopes in Quaternary soil carbonates as indicators of ecogeomorphic changes in the northern Chihuahuan Desert, USA. *Geoderma* 82, 137–172. doi:10.1016/s0016-7061(97)00100-6
- Monger, H. C. (2014). "Soils as generators and sinks of inorganic carbon in geologic time," in *Soil carbon*. Editors A. E. Hartemink and K. McSweeney (Cham: Springer), 27–36.
- Monnin, E., Steig, E. J., Siegenthaler, U., Kawamura, K., Schwander, J., Stauffer, B., et al. (2004). Evidence for substantial accumulation rate variability in Antarctica during the Holocene through synchronization of CO_2 in the Taylor Dome, Dome C and DML ice cores. *Earth Planet. Sci. Lett.* 224, 45–54. doi:10.1016/j.epsl.2004.05.007
- Netterberg, F. (1971). Calcrete in road construction, NIRR BULL 10. *CSIR Res. Rep.* 266, 56.
- Netterberg, F. (1978). Dating and correlation of calcretes and other pedocretes. *Trans. Geol. Soc. S. Afr.* 81, 379–391.
- Novák, V., and Hlaváčiková, H. (2019). *Applied soil hydrology*. Cham: Springer.
- Oerter, E. J., Amundson, R., Heimsath, A., Jungers, M., Chong, G., and Renne, P. (2016). Early to middle miocene climate in the Atacama Desert of northern Chile. *Palaeogeogr. Palaeoclimatol. Palaeoecol.* 441, 890–900. doi:10.1016/j.palaeo.2015.10.038
- Orland, I. J., Bar-Matthews, M., Ayalon, A., Matthews, A., Kozdon, R., Ushikubo, T., et al. (2012). Seasonal resolution of eastern mediterranean climate change since 34 ka from a Soreq cave speleothem. *Geochim. Cosmochim. Acta.* 89, 60–71. doi:10.1016/j.gca.2012.04.035
- Pendall, E., Harden, J., Trumbore, S., and Chadwick, O. (1994). Isotopic approach to soil carbonate dynamics and implications for paleoclimatic interpretations. *Quat. Res.* 42, 60–71. doi:10.1006/qres.1994.1054
- Petrie, C. A., and Weeks, L. (2019). "The Iranian plateau and the indus river basin," in *Climate changes in the Holocene, impacts and human adoption*. Editor E. Chiotis (Boca Raton, FL: CRC Press), 293–325.
- Poesen, J., and Lavee, H. (1994). Rock fragments in top soils: Significance and processes. *Catena* 23, 1–28. doi:10.1016/0341-8162(94)90050-7
- Pustovoytov, K. (1998). Pedogenic carbonate cutans as a record of the Holocene history of relic tundra-steppes of the Upper Kolyan Valley (North-Eastern Asia). *Catena* 34, 185–195. doi:10.1016/s0341-8162(98)00088-5
- Pustovoytov, K. (2003). Growth rates of pedogenic carbonate coatings on coarse clasts. *Quat. Int.* 106–107, 131–140. doi:10.1016/s1040-6182(02)00168-4
- Quade, J. (2014). The carbon, oxygen, and clumped isotopic composition of soil carbonate in archaeology. *Treat. Geochem.* 14, 129–143. doi:10.1016/B978-0-08-095975-7.01211-0

- Railsback, L. B. (2021). Pedogenic carbonate nodules from a forested region of humid climate in central Tennessee, USA, and their implications for interpretation of C3-C4 relationships and seasonality of meteoric precipitation from carbon isotope ($\delta^{13}\text{C}$) data. *Catena* 200, 105169. doi:10.1016/j.catena.2021.105169
- Rashidi, Z., Murray, A., Khormali, F., Farpoor, M. H., Karimi, A., and Sohbati, R. (2022). Late pleistocene-holocene pedogenesis and palaeoclimate in Western Asia from paleosols of the central Iranian plateau. *Boreas* 51 (1), 201–218. doi:10.1111/bor.12541
- Reimer, P. J., Bard, E., Bayliss, A., Beck, J. W., Blackwell, P. G., Ramsey, C. B., et al. (2013). Selection and treatment of data for radiocarbon calibration: An update to the international calibration (IntCal) criteria. *Radiocarbon* 55, 1923–1945. doi:10.2458/azu_js_rc.55.16955
- Reimer, P. (2020). Composition and consequences of the IntCal20 radiocarbon calibration curve. *Quat. Res.* 96, 22–27. doi:10.1017/qua.2020.42
- Retallack, G. J. (1994). "The environmental factor approach to the interpretation of paleosols." *Factors of soil formation: A fiftieth anniversary retrospective*. Editors R. G. Amundson, J. W. Harden, and M. J. Singer (Madison, WI: Soil Science Society of America Special Publication), 33, 31–64.
- Retallack, G. J. (2005). Pedogenic carbonate proxies for amount and seasonality of precipitation in paleosols. *Geology* 33, 333–336. doi:10.1130/g21263.1
- Romanek, C. S., Grossman, E. L., and Morse, J. W. (1992). Carbon isotopic fractionation in synthetic aragonite and calcite: Effects of temperature and precipitation rate. *Geochim. Cosmochim. Acta*. 56, 419–430. doi:10.1016/0016-7037(92)90142-6
- Rozanski, K., Araguás-Araguás, L., and Gonfiantini, R. (1992). Relation between long-term trends of oxygen-18 isotope composition of precipitation and climate. *Science* 258, 981–985. doi:10.1126/science.258.5084.981
- Saadatmand, G. (1999). *Reconnaissance soil survey and land classifications of central Isfahan province (Kouhpaye and Segzi)*. Tehran, Iran: Soil and Water Research Institute of Iran, Publication No. 1094, 65. (in Persian).
- Sarangi, V., Agrawal, S., and Sanyal, P. (2021). The disparity in the abundance of C₄ plants estimated using the carbon isotopic composition of paleosol components. *Palaeogeogr. Palaeoclimatol. Palaeoecol.* 561, 110068. doi:10.1016/j.palaeo.2020.110068
- Schaffernicht, E. J., Ludwig, P., and Shao, Y. (2020). Linkage between dust cycle and loess of the last glacial maximum in Europe. *Atmos. Chem. Phys.* 20, 4969–4986. doi:10.5194/acp-20-4969-2020
- Schmidt, A., Quigley, M., Fattahi, M., Azizi, G., Masghsoudi, M., and Fazeli, H. (2011). Holocene settlement shifts and palaeoenvironments on the Central Iranian Plateau: Investigating linked systems. *Holocene* 21 (4), 583–595. doi:10.1177/0959683610385961
- Schoeneberger, P. J., Wysocki, D. A., Benham, E. C., and Broderick, W. D. (2012). *Field book for describing and sampling soils*. Washington DC: Natural Resources Conservation Service, United States Department of Agriculture.
- Shankar, N., and Achyuthan, H. (2007). Genesis of calcic and petrocalcic horizons from Coimbatore, Tamil Nadu: Micromorphology and geochemical studies. *Quat. Int.* 175, 140–154. doi:10.1016/j.quaint.2007.05.017
- Sharifi, A., Pourmand, A., Canuel, E. A., Ferer-Tyler, E., Peterson, L. C., Aichner, B., et al. (2015). Abrupt climate variability since the last glaciation based on a high-resolution, multi-proxy peat record from NW Iran: The hand that rocked the Cradle of Civilisation? *Quat. Sci. Rev.* 123, 215–230. doi:10.1016/j.quascirev.2015.07.006
- Sharififar, A., Minasyan, B., Arrouays, D., Boulonne, L., Jang, H. J., Mcbratney, A., et al. (2023). Soil inorganic carbon, the other and equally important soil carbon pool: distribution, controlling factors, and the impact of climate change. *Adv. Agron.* 178, 165–231.
- Sheldon, N. D., and Tabor, N. J. (2009). Quantitative paleoenvironmental and paleoclimatic reconstruction using paleosols. *Earth-Sci. Rev.* 95, 1–52. doi:10.1016/j.earscirev.2009.03.004
- Sheldon, N. D. (2006). Abrupt chemical weathering increase across the Permian-Triassic boundary. *Palaeogeogr. Palaeoclimatol. Palaeoecol.* 231, 315–321. doi:10.1016/j.palaeo.2005.09.001
- Shlomon, R. J. (1978). *Preliminary Quaternary geology/soil-stratigraphy proposed nuclear power plant (NPPI) Isfahan Iran, (Newport Beach, California)*. Roy J. Shlomon and Associates, Inc.
- Shoaei, M. J., Breeze, P. S., Drake, N. A., Hashemi, S. M., Vahdati Nasab, H., Breitenbach, S. F. M., et al. (2023). Defining paleoclimatic routes and opportunities for hominin dispersals across Iran. *Plos One* 18 (3), e0281872. doi:10.1371/journal.pone.0281872
- Soil Survey Staff (2014). *Kellogg soil survey laboratory methods manual*. Washington DC: Natural Resources Conservation Service, United States Department of Agriculture.
- Soleimani, M., Nadimi, A., Koltai, G., Dubyansky, Y., Carolin, S., and Spotl, C. (2023). Stalagmite evidence of Last Glacial Maximum to early Holocene climate variability in southwestern Iran. *J. Quat. Sci.* 38 (3), 308–318. doi:10.1002/jqs.3478
- Thomas, D. S. G., Bateman, M. D., Mehrshahi, D., and O'hara, S. L. (1997). Development and environmental significance of an eolian sand ramp of last-glacial age, central Iran. *Quat. Res.* 48, 155–161. doi:10.1006/qres.1997.1923
- Tierney, J. E., Poulsen, C. J., Montañez, I. P., Bhattacharya, T., Feng, R., Ford, H. L., et al. (2020). Past climates inform our future. *Science* 370, eaay3701. doi:10.1126/science.aay3701
- Torfstein, A., Goldstein, S. L., Stein, M., and Enzel, Y. (2013). Impacts of abrupt climate changes in the Levant from last glacial Dead Sea levels. *Quat. Sci. Rev.* 69, 1–7. doi:10.1016/j.quascirev.2013.02.015
- Wang, Y., Amundson, R., and Trumbore, S. (1994). A model for soil ¹⁴C and its implications for using ¹⁴C to date pedogenic carbonate. *Geochimica Cosmochimica Acta* 58, 393–399. doi:10.1016/0016-7037(94)90472-3
- Yaalon, D. H. (1997). Soils in the mediterranean region: What makes them different? *Catena* 28, 157–169. doi:10.1016/s0341-8162(96)00035-5
- Yanes, Y., Wold, D., and Faust, D. (2019). Paleoenvironmental reconstruction and sedimentary processes in drylands. *Quat. Res.* 91, 1–3. doi:10.1017/qua.2018.126
- Yang, Q. L., and Jing, G. (2022). *Reconstruction of the paleoclimate from valikhanov loess sequence in central Asia arid zone since 32 ka through N-alkane biomarker analysis*. SSRN. doi:10.2139/ssrn.4072913
- Zahedi, M. (1976). *Explanatory text of the esfahan quadrangle map 1:250000*. Tehran: Geological Society of Iran.
- Zamanian, K., Pustovoytov, K., and Kuzyakov, Y. (2016). Pedogenic carbonates: Forms and formation processes. *Earth-Sci. Rev.* 157, 1–17. doi:10.1016/j.earscirev.2016.03.003
- Zhou, R., Wen, X., Lu, L., Li, Y., and Huang, C. (2021). Holocene paleosols and paleoclimate for the arid upper Minjiang River valley in the eastern Tibetan Plateau. *Catena* 206, 105555. doi:10.1016/j.catena.2021.105555